Instituto Tecnológico y de Estudios Superiores de Monterrey

Campus Monterrey

School of Engineering and Sciences

Data-Driven Control of Voltage Source Converters for AC/DC Power Grids

A dissertation presented by

David Rivera

Submitted to the
School of Engineering and Sciences
in partial fulfillment of the requirements for the degree of

Doctor of Philosophy
in
Engineering Science

Major in Electrical Engineering

Monterrey Nuevo León, June 15th, 2022

Instituto Tecnológico y de Estudios Superiores de Monterrey

Campus Monterrey

School of Engineering and Sciences

The committee members, hereby, certify that have read the thesis presented by David Rivera and that it is fully adequate in scope and quality as a partial requirement for the degree of Doctor of Philosophy in Engineering Science, with a major in Electrical Engineering.

Dr. Daniel Guillén Aparicio
Tecnológico de Monterrey
Principal Advisor

Dr. Jonathan C. Mayo-Maldonado
The University of Sheffield
Co-advisor

Dr. Armando Llamas Terres
Tecnológico de Monterrey
Committee member

Dr. Federico Viramontes Brown
Tecnológico de Monterrey
Committee member

Dr. Jesús E. Valdez Resendiz
Tecnológico de Monterrey
Committee member

Dr. Rubén Morales Menéndez
Dean of Graduate Studies
School of Engineering and Sciences

Monterrey Nuevo León, June 15th, 2022

Dedication

Dedicated to my parents, Gladys and Armando, whose love, motivation and support have been fundamental in this journey. To my beloved brothers and sister, Daniel, Armando and Sara, for the unconditional support.

Acknowledgements

I want to express my most sincere thanks:

To Dr. Daniel Guillén, for his invaluable encouragement and patience. The invaluable support and guidance from Dr. Daniel made this research work possible.

To Dr. Jonathan Mayo, for the guidance and support.

To my professors, Dr. Armando Llama, Dr. Federico Viramontes and Dr. Jesús Valdez for sharing their knowledge and supporting me during this long journey and also for being members of the committee.

To my PhD colleagues, Javier, Juan Carlos and Carlos, for the support, motivation and the marvelous moments we shared.

To Jenny Medina, for her love, dedication and supportive attitude at all times. From the first time I met her, she was one of the nicest person I have ever met.

To my teacher and guide, Dr. Osvaldo Micheloud for giving me the opportunity and support to start this PhD.

To CONACYT, México and Tecnológico de Monterrey for providing the funds and making this journey possible.

ABSTRACT

The use of Voltage Source Converters (VSC) is gaining ground in recent years due to the many benefits it offers. A wide range of electronic devices are using this technology, including systems like renewable energy sources (RES), direct current transmission, Flexible AC transmission system (FACTS), are some of which can be mentioned. The energy matrixes of the countries around the world are changing and the electrical power systems are experiencing new challenges in control, dispatch, design, etc.

This thesis involves the design of a new type of controller for VSC. This new controller is based on data gathered from the simulation of multiple setpoints of operations of a model-based control used for a VSC connected to the grid. Before the design of this new data-driven control, an model-based controller is modelled and tuned according to grid parameters and dynamic characteristics.

The design of the new controller starts from the data obtained from the previous simulations of the model-based controller. The data is used as input to the control design which is based on the measured variables (time-discrete data). The control design follows many particular criteria defined by the control theory and can be solved by an optimization approach in order to comply with the stability function. The new controller must meet certain parameters such as robustness, speed, stability criterion, and capturing the grid dynamic characteristics within itself.

The tests to compare the performance between the data-driven controller and model-based controller consist of using three types of devices that are VSC-based. These tests include step response, voltage recovery under transient conditions due to fault and load shedding. With these comparisons, the perks and disadvantages of using the new control approach were presented and proven using a two-area, four generator electric power system.

Contents

List of Tables

List of Figures

Chapter 1

Introduction

This chapter gives a brief overview of voltage source converters (VSC) employed in power transmission in direct current (DC), and flexible alternating current transmission system (FACTS) as well as their influence on modern electric power systems.

1.1 Motivation

The current growth in the electricity demand and the need for long distances transmission requires the use of high voltage to achieve efficient and reliable energy quality. For this reason, the concurrence of high voltage direct current (HVDC) systems with AC systems has generated a technological evolution, turning them into products of high reliability and efficiency, thus acquiring great importance in the transmission of electrical energy.

The reliability of power transmission systems has always been an essential topic of discussion leading to different areas of study. There are many studies that have been conducted to determine the feasibility of a more robust and stable power grid when experiencing failures. There have also been studies focused on increasing efficiency, as well as reducing costs and losses in power systems. An area of opportunity has been the use of HVDC systems to transmit large amounts of power over long distances with

advantages such as lower losses due to the Joule effect (skin effect), better response to failures, and independent control of active and reactive power, etc.

One of the most important features of HVDC and FACTS deals with the fact that reactive power and real power can be controlled independently within a couple of milliseconds due to the fast switching of the power converters which brings the opportunity for improving the transient stability. Like any other system, an electric power system tends to suffer from failures. These can be either short circuits, load tripping, generation disconnection/connection, or any other event that alter the steady-state of the system. An external event can cause serious damage to an electric power system and can affect the entire operation. As a consequence of that, transient stability should be guaranteed to maintain an energy balance between the generated power and the demanded power. Indeed, some power system components may help improve the dynamic response of the system based on the controllers used. Therefore, there is special attention to VSC and its control to enhance the grid's dynamic under transient conditions.

Prompted by the need to conduct dynamic simulations in large power system with VSC, the dynamic behavior of the full grid will depend on many variables according to the operating point. The optimal operation of VSC involves many variables, among which can mention the tuning of its internal control, which will determine the response speed to maintain a stable state in case of a perturbation. Since the control system of a VSC is complex, non-linear in other words, the tuning of its controls in many cases leads to the need for linearization. The linearization of systems such as the VSC can generate a satisfactory tuning in many cases, but there are some assumptions made, for example, the interconection between a VSC and the electrical grid is carried out by an impedance and the grid is represented as an infinite bus. An infinite bus lacks of information and physical properties of an electrical grid, ranging from power injection limitations, ramp rate power injection, voltage regulation, etc. Another essential issue about linear system regarding power ystem is associated with the dynamic power equiment such as generators, loads etc. The equivalent model of an generator depends

on different factors such as type of generator, exciter, power system stabilizer (PSS), automatic voltage regulator (AVR) and many others. All the aspects previously mentioned are not taken in consideration during the linearization of the converter when an infinite bus is used.

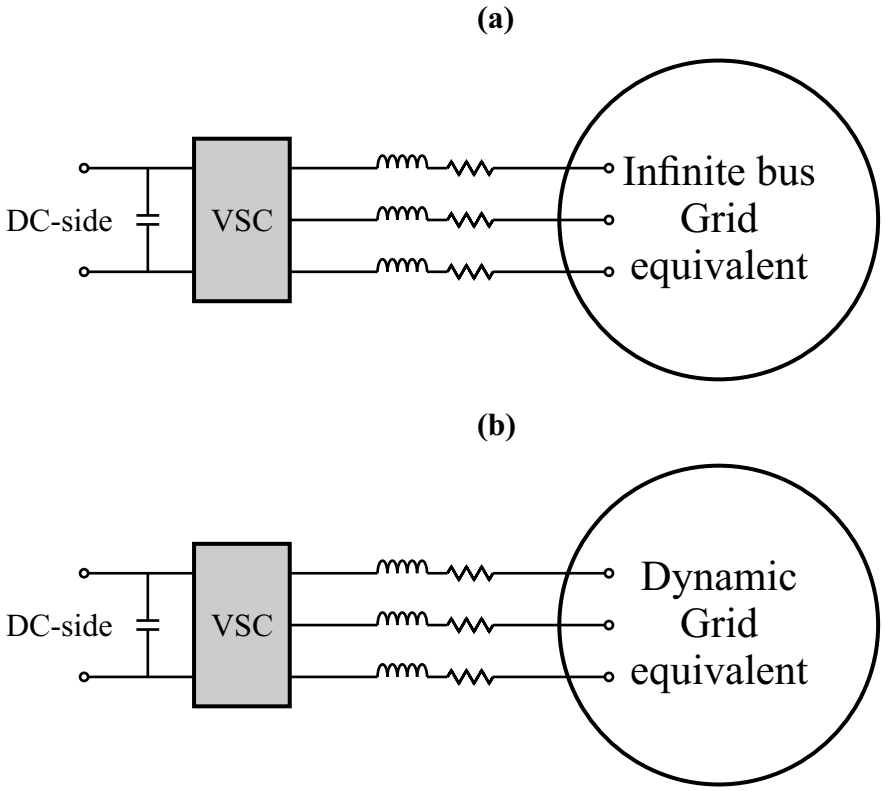

Figure 1.1: Infinite bus grid equivalent vs dynamic grid equivalent

The linearization of a VSC for tuning purposes may give a reliable approximation, but the optimal performance might not be guaranteed. Fig. 1.1 shows two different types of grid equivalents. In the past few years, there have been multiple approaches to perform a suitable tuning for the VSC control that offered good results, but what if the controller can capture the dynamic characteristics of the entire grid, including the generators, and can be scalable to multiple types of devices based on VSC?. The main motivation of this thesis is to develop a new controller prompted by a data-driven approach; the controller must meet certain parameters such as robustness, speed, stability criterion, and capturing the grid dynamic characteristics within itself. Many studies have already focus on data-driven to create auxiliary controls to enhance the

model-based controller, but none has entirely used a controlled to replace the entire control system being this the main target of this work.

1.2 State-of-the-art

The electricity supply plays an indispensable role in today's society. The use of energy became a basic need of societies and is a key element in the development of countries. The use of electrical energy is entirely employed by households, industry, commerce, or other complex activities such as space exploration. Without any doubt, this has become a fundamental part of our lives since it has changed people's activities in many ways. Specifying precisely who invented electricity would be impossible, but contributions from many scientists over time have helped to understand how it works. From its generation, transmission, distribution, and consumption; electrical power systems appear to be simple, but in reality, they are not. These systems are considered the largest that exist and given their size, one of the most complex.

Scientists such as Nikola Tesla and Thomas Alba Edison were of fundamental importance in the development of the structure that made electrical energy usable, from its generation to its consumption. It is clear to mention that behind all the theory that describes how electricity works, from the simplest concept such as Coulomb's Law of forces to the electromagnetic theory, was a joint effort by several scientists who over the years developed mathematical models; Maxwell's laws for example, that allow us to model and understand energy. This knowledge made possible the design such as, for example, the electric generator, and later more complex systems such as the electric power systems. All these inventions had several people involved with many different points of view. One of the most famous cases was the conflict called "The War of the Currents." This conflict was a debate about which type of system, alternating current (AC) or direct current (DC), was more appropriate to use in energy transmission. On one side, Nikola Tesla proposed the AC system that was more suitable for energy transmission, and on the other side, Thomas Alba Edison

proposed a DC system for the same purpose. In the end, AC prevailed and has dominated ever since. In economic and technical terms AC power system is more auspicious compared to DC power systems. From the intrinsic simplicity of voltage step-up or step-down to the three-phase generation (DC generators are more complex and expensive), the AC power system seems to overcome DC transmission systems in every aspect.

The use of DC systems for transmission has been limited throughout the years mainly by the lack of power converters rating and voltage limitation. The development of the mercury valves created a new opportunity for the use of DC on transmission systems. But mercury valves' power and voltage rating were very limited. With the invention of the transistor, new transmission opportunities opened up such as HVDC and FACTS. Transistors replaced mercury valves with better performance such as greater power conversion, higher voltages ratings, and faster switching speeds. But the technology had a maturing process that now allows developing projects of power transmission based on HVDC, static compensators and energy storage.

1.2.1 Types of converters

The invention of the mercury vapor valve gave an essential boost in AC/DC conversion [30]. In 1933 U. Lamm developed the first high-voltage mercury valve converter based on the valve developed by P. Cooper in 1903 [2]. The mercury vapor-based rectification technology was used in power transmission, and industrial processes from 1930 to 1975 [30] after that the technology became obsolete, which was later replaced by thyristor valves [2].

Nowadays, there are two dominant methods in converting AC power to DC and vice versa. Both methods use power electronic converters, and these are the voltage source converter VSC and the line commutated converter LCC (CSC) [30]. The VSC makes use of the IGBT transistors and the LCC for its part, of the thyristors. Thyristors (LCC converters) are capable of handling higher powers than IGBT (VSC), that

is, the largest HVDC transmission projects are LCC systems (CSC). A comparative example is two of the HVDC transmission projects in 2014. In Xiluodu-Zhejiang, China, an HVDC line from 8.0 GW to +-800 kV with LCC-HVDC technology was planned, and in that same year, in Norway, one of 0.7 GW ± 500 kV with VSC technology [2]. The DC link in China represents 15% of the installed capacity in Mexico, which is 54.85 GW [7]. Thyristors are solid-state silicon semiconductor devices that consist of four alternating layers of N and P material. They function as a bi-stable switch. They conduct when a pulse of current is applied to the gate, remaining active until the voltage is reversed [2].

In 2000 the Insulated-Gate Bipolar Transistor IGBT was introduced. This transistor has three layers of N and P material. They are made of silicon and are capable of withstanding greater power than other transistors, such as the BJT. The development of the IGBT occurred in the 80s, and in the late 90s it became for using commercially. IGBTs are devices of high efficiency and interruption speed [2]. Unlike thyristors, IGBT can be turned on and off at the desired time without having to reach the voltage polarity reversal. IGBTs became the key component for modern VSC because of their switching speed and high power and voltage capabilities.

1.2.2 VSC applications and advantages

VSC has multiple applications and advantages compared to similar technologies. Due to the many applications, VSC is usually divided into two main groups: HVDC transmission and Flexible AC Transmission Systems FACTs. When a VSC is used for power transmission using HVDC, one can find some of the following advantages:

- Reduced right-of-way width for overhead transmission compared to High voltage alternating current (HVAC) transmission.
- Real and reactive power independent control.
- Lower losses over long distances.

- Connection of asynchronous systems whether if a back-to-back of DC link configuration is used.
- Black start capability compared to LCC.
- Enables underground and submarines transmission over long distances.
- Voltage control on buses which helps to enhance the overall system stability under transient conditions.

Considering VSC as FACTS:

- VSC capability to deliver reactive power when needed brings better voltage control.
- Active power can be stored using batteries and can be injected to the grid by the VSC, which under certain conditions should improve the power system stability.
- VSC can improve the frequency control of the grid by delivering active power when unbalance conditions exist between power generation and demand.
- Voltage control done by the VSC improves voltage regulation.
- With an improved voltage regulation, reactive power loss due to transmission can be decreased.
- Optimal power flow related to optimal power dispatch can be controlled better.

A VSC system allows independent control of real and reactive power, which is one of the major features of this technology. The injection of reactive power to the grid contributes to maintaining the voltage profile in an established range, this offers controllability to the power flows of transmission lines, and helps enhance the power system stability under transient conditions. Optimal power flow is an essential tool for solving the economical dispatch problem, and VSC by means of HVDC transmission allows controlling the real power flow through the DC line as long as needed. Power

lines congestion is another common problem in the economical dispatch problem, and VSC-HVDC transmission is well suited to manage power flow when the AC lines are congested. On the other hand, transmission using LCC-HVDC is normally used for bulk power transmission because of its lower losses over long distances compared to AC transmission.

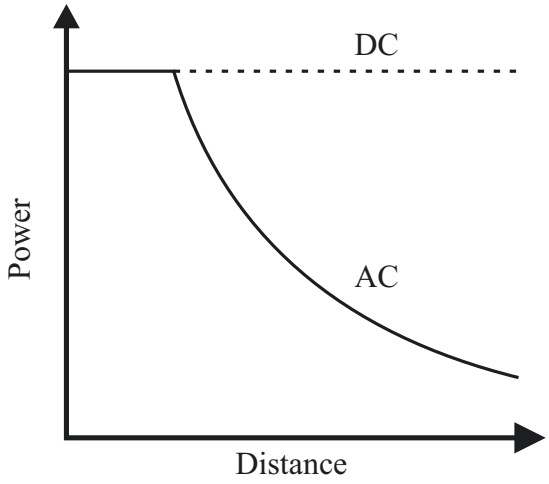

Figure 1.2: AC compared to DC power losses over distance

Even though LCC doesn't provide independent power control, nowadays it is used all over the world. AC power transmission experiences a phenomenon called *"skin effect"* which limits the current to travel near the surface of the conductor, increasing the electrical resistance as shown in Fig.1.3. More electrical resistance means more power loss due to *"Joule effect"*. Direct current transmission does not experience this type of physical effect, so the current travels in a uniformly distributed way through the conductor, therefore the losses due to resistance are less compared to an equivalent alternating current system. Fig.1.2 shows the comparison between AC and DC power transmission losses over distance.

VSC-HVDC enables power transfer between two asynchronous systems. Power systems around the globe are continuously growing tending to create bigger grids by the interconnection of small to large grids trying to avoid "islanding". Creating a large grid is beneficial to the overall stability of the system and improves the economical dispatch, but sometimes power systems don't have the same frequency or phase.

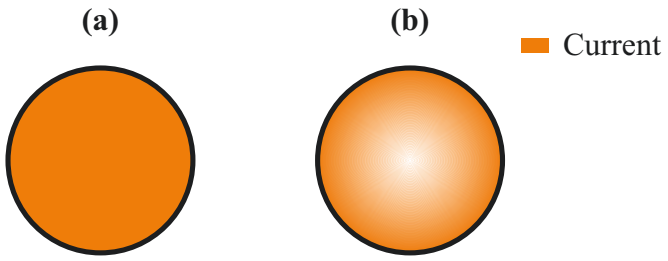

Figure 1.3: Cross-section of a conductor: (a) DC current, (b) AC current

HVDC allows the connection of every of these small or large grids contributing to build an integrated grid.

AC underground or submarine power transmission is suitable for short distances. Insulated conductors, called cables, in underground and submarine systems require a material that contains the electric field and isolates it from physical contact with the external environment. The structure of an HVDC cable is usually very similar to that of an HVAC cable. In general, the designs of HVDC cables do not vary according to their manufacturer, but the types of materials that are used for their manufacture do, mainly insulating and semiconductor materials.

FACTs are becoming essential in modern electrical grids. New types of energy generation like renewable sources, brought new challenges to conventional grids. FACTS provide fast dynamic capabilities improving voltagea, and frequency stability [31]. FACTS encompass a series of devices based on VSC with different purposes. These devices, depending on its type, can provide voltage control, reactive power injection, and active power injection giving extra support to the grid by improving stability.

1.2.3 Flexible AC Transmission Systems (FACTs)

Flexible AC Transmission Systems (FACTS) are static components, usually power electronic-based devices, used in AC system to increase power transfer capacity and to enhance the power system stability [34]. FACTS increases the voltage control utilizing fast active/reactive power injection which contributes to improve optimal

power flow and power dispatch. Voltage control, besides of improving the economic operation, it also creates more stable and reliable systems. When any power system suffers from an external event such as faults, connection/disconnection of loads, etc.; the system tends to return to a new steady state that needs fast power injection. This is possible by employing STATCOM, SVC, BESS and other types of FACTS devices.

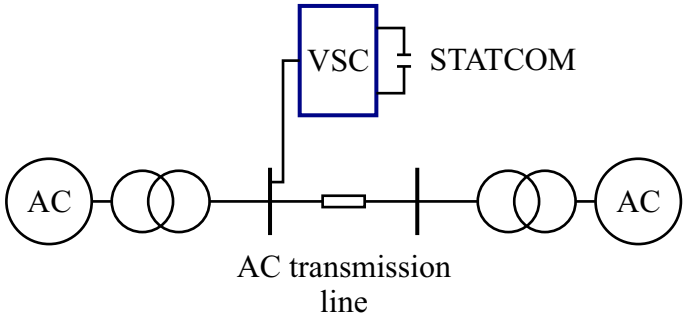

Figure 1.4: STATCOM connected to a small electric grid

STATCOMs are VSC-based and operate as a reactive synchronous generator. The main objective of a STATCOM is the injection or absorption of reactive energy, which helps to improve various aspects of the grid, such as increasing bulk energy transmission, voltage control, and in some cases, it can be used to enhance transient stability and power oscillation damping [11]. A STATCOM is connected in parallel to the grid usually on or close to substations. STATCOMs absorb a minimum quantity of active power for compensating the active power losses within themselves and to maintain a desired DC voltage on the DC-side. Even though these types of systems cannot provide virtual inertial to the system by injection of active power, their benefits to maintaining the voltage profile during transient conditions are extremely beneficial to the reliability of the grid.

Another widely used type of FACT is the Battery Energy Storage Systems (BESS). BESS is VSC-based just like STATCOM and operates in a similar way with some differences. BESS can provide active power by means of battery energy storage and also provides voltage control by reactive power injection. With the penetration of renewable energy sources increasingly accentuated into conventional networks, the rotational inertia of the system has decreased, so it is necessary to create mecha-

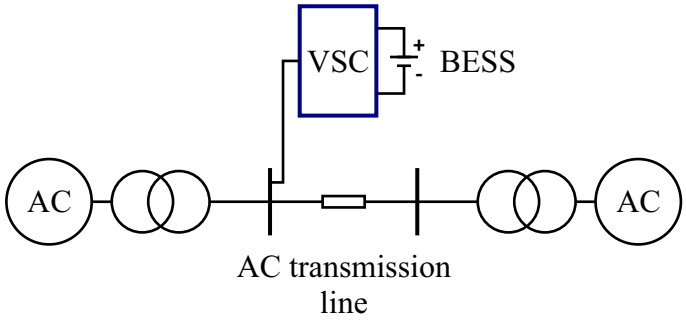

Figure 1.5: BESS providing active and reactive power support to an electric grid

nisms/devices that provide a rapid injection of active power, such as BESS because this can be used to create virtual inertia that the system is lacking when the system is under transient conditions. FACTs and HVDC transmission are increasingly being implemented across modern electric grids. Power grids are continuously changing and expanding, there is a need for new solutions in order to make reliable networks. FACTS devices open new opportunities for the enhancement of AC grids. Advantages such as voltage control by means of reactive power injection, virtual rotational inertial, increased power transfer, and power oscillation damping improvement make FACTs an important niche in future power grids.

1.2.4 HVDC transmission

The advances in research and cost reduction in the area of power electronics have pushed for opting for the use of power electronic converters in many countries to complement the transmission in alternating current. Lower active power losses due to skin effect, electronic reactive power control, better stability performance, the connection of asynchronous systems, and underwater lines, are some advantages of HVDC-based transmission systems. HVDC systems typically consist of two terminals with converter stations at each end, one terminal that converts from AC to DC (rectifying station), and another terminal at the receiving point from DC to AC (inverting station) [29]. The two ends of the converters are connected through DC transmission lines which can be aerial, underwater, underground, or buses if they are

contiguous (back-to-back configuration) [30]. The development and progress of HVDC technology have depended on two factors: cables and power electronics. That involves the manufacture of highly efficient semiconductors for the topology of converters [13] and the development of materials (polymers, additives, semiconductors, etc.) for transmission lines.

1.2.5 Line Commutated Converter (LCC)

Conventional HVDC transmission systems use LCCs (Line commutated converters) in their conversion process. The LCCs switch through thyristor valves through synchronous and stable voltage to operate [3]. LCC technology is currently capable of handling the highest voltage and power in HVDC systems [30]. The basic building block of a conversion system is three-phase, with a full-wave bridge called the six-pulse or Graetz bridge, as it performs 6 switches in each cycle. But in a real scenario, two 6-pulse bridges are used on each terminal, which makes it a 12-pulse operation as shown in Fig.1.6. This is because when two six-pulse bridges are used, the DC voltage can be increased and certain characteristic harmonics can be eliminated in the AC current and DC voltage [3]. For example, a LCC technology using 12-pulse bridges generates harmonics of order $12n \pm 1$ and $12n$ in the DC voltage and AC current [13], for this reason it is necessary to use harmonic filters synchronized to the characteristic values.

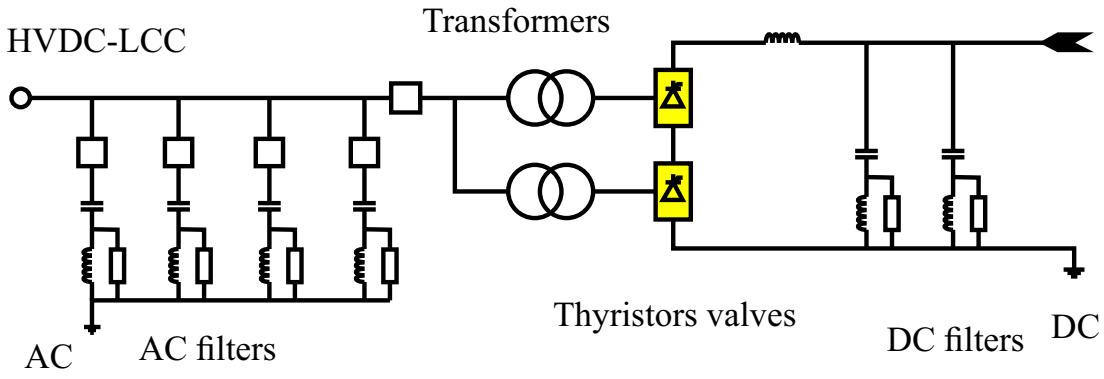

Figure 1.6: LCC station used for HVDC transmission

1.2.6 Voltage Source Converter (VSC) basic structure

VSC applications are diverse. A high-power converter it can be used for transmission, which is called VSC-HVDC transmission, it also can be employed to compensate reactive power through Static Synchronous Compensator (STATCOM) and it can also compensate both, real and reactive power through a Battery Storage Energy Systems (BESS). VSC also plays an essential role in renewable energy sources (RES) like photovoltaic and wind generation. The operation for each application may vary but the structure of the converter remains similar.

Voltage source converter-based HVDC technology uses typically IGBTs (isolated gate bipolar transistors), which are fully controllable switches, which means that they can be opened and closed when desired. Depending on the type of topology, the converter can have many levels. Figure 1.7 depicts a VSC station which includes other components.

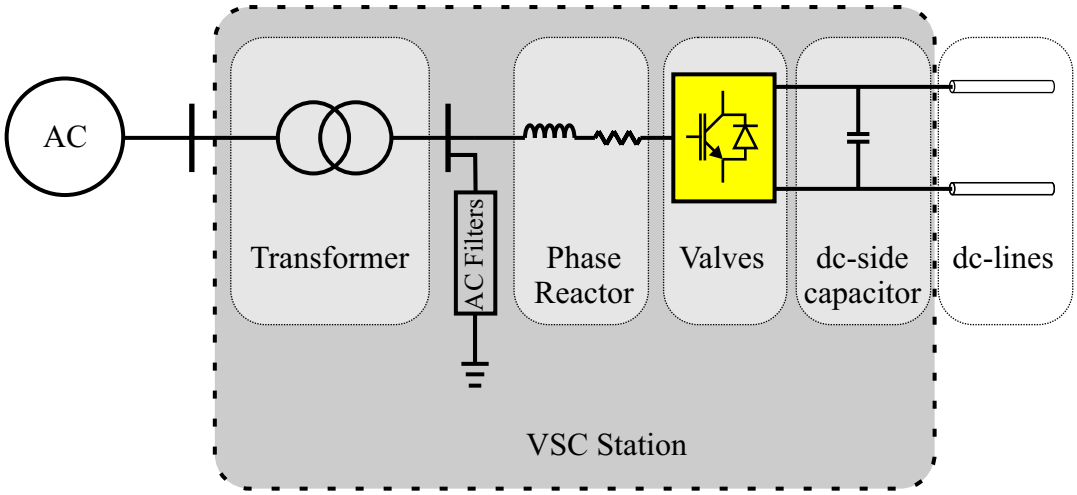

Figure 1.7: VSC station used for HVDC transmission

AC-side transformer

The VSC is usually connected to the network via a transformer. Depending on the three-phase connection it is used to block some harmonics going to the main block

due to the valves. The AC-side transformer is also used to match the different rated values of the AC network and the VSC.

Phase reactor

The coupling impedances between the network and the converter must be large enough to minimize current variations caused by the switching of the converter and have to be small enough so that the voltage drop can be considered negligible. Typical values are 0.15 and 0.20 per unit (p.u.) values [10]. The coupling impedances allow power control.

AC-side filters

The filters must guarantee the quality of both voltage and current, canceling or reducing harmonics. The filters are calculated based on the harmonic spectrum generated by the converter and the size of the coupling impedance.

Valves and bridge

The controllable switches (IGBTs) in the VSC allow the converter to generate a desired alternating voltage. The VSC can control magnitude and phase, that is, it can control the real and reactive power independently. This advantage over the conventional LCC-HVDC gives VSC the opportunity to perform better during a perturbation (fault, connection/disconnection of load, etc.). The VSC uses the Pulse Width Modulation (PWM) to generate a sinusoidal output signal.

The most basic operation of a VSC starts from the fundamental half-bridge converter as shown in Fig. 1.9(a) [36]. The AC side is connected to the DC side by a bridge of IGBTs and capacitors which have the following sequence according to Fig. 1.9(b) [36]:

(a)

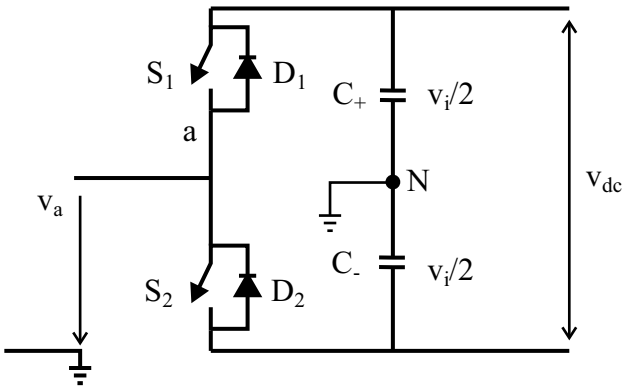

Figure 1.8: Half-Bridge scheme

(b)

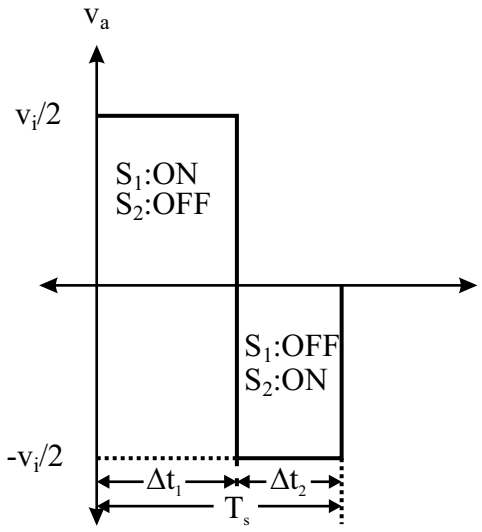

Figure 1.9: Half-Bridge output signal

1. There's a pattern which is periodic and has a defined frequency as well a period.

2. When S_1 is on, S_2 is off and the output V_a becomes $V_{dc}/2$ with a period of Δt_1.

3. When S_2 is on, S_1 is off and the output V_a becomes $-V_{dc}/2$ with a period of Δt_2.

Figure 1.10 shows the scheme for a three-phase system whose operation is quite

similar to the half-bridge but now with 6 IGBTs (switches).

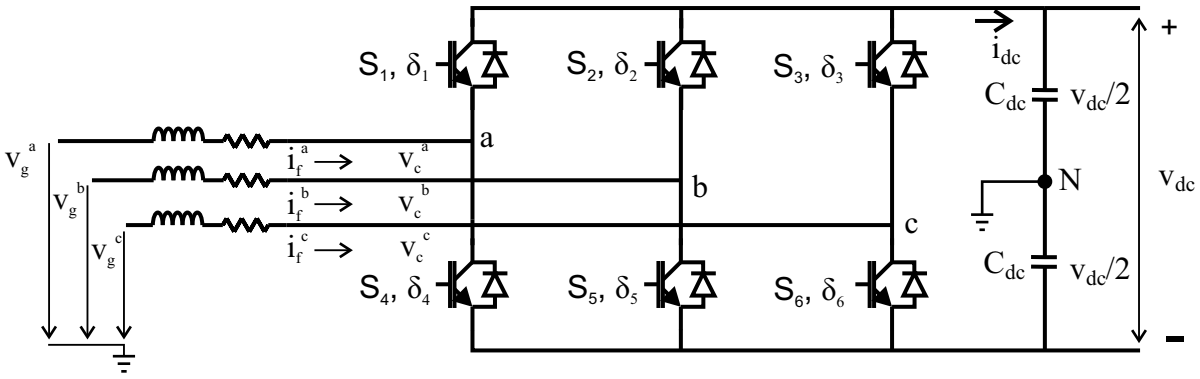

Figure 1.10: Full-Bridge three-phase scheme

The fundamental voltage on the AC-side is controlled by pulse-width modulation (PWM) [39]. The switches are triggered by a modulation signal which depends on a carrier signal (usually 2000 Hz or a larger frequency) [39] and a reference signal (with the same frequency as the output signal). The maximum or minimum output voltage of the converter for each phase V_c^{abc} is defined by $V_{dc}/2$ and $-V_{dc}/2$, respectively, as shown in Fig. 1.11. The average VSC model considers the modulation signal $m(t)$, which is constant during one switching cycle [18]. Taking into consideration the previous assumption the converter average voltage is defined as:

$$v_c = \frac{1}{T_s} \int_{t-T_s}^{t} V_c(\tau)\, d\tau \tag{1.1}$$

where v_c is the average converter voltage and T_s the modulation signal period.

If the switching frequency is much higher than the modulation signal frequency, an average converter can be used and the relationship between AC and DC is the following [18]:

$$v_c = m(t)\frac{U_{dc}}{2} \tag{1.2}$$

The modulation signal $m(t)$ can be expressed as (phase A)[37] :

$$ma(t) = M_a \cos(\omega t + \psi_m) \tag{1.3}$$

where M_a is the reference signal, ω represents the angular frequency of the system and ϕ is the angle.

The fundamental component AC voltage (line-to-ground) of phase A can be expressed in what follows [37]:

$$v_{a01} = \frac{1}{2} v_{dc} m_a v_{a01} = \frac{1}{2} v_{dc} M_a \cos(\omega t + \psi_m) \tag{1.4}$$

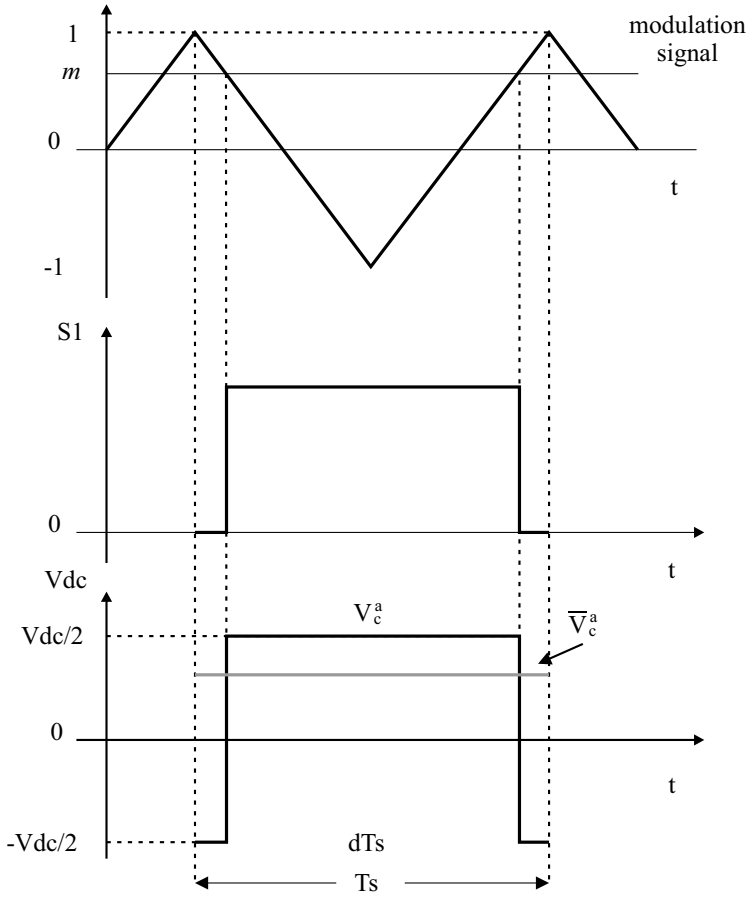

Figure 1.11: Modulation

1.2.7 Sinusoidal Pulse-Width Modulation (SPWM) for three-phase two level converters

SPWM is a type of PWM that uses a sine signal as a reference signal and a triangular signal as a carrier signal as shown in Fig1.13. Even though there are more complex systems that employ multilevel converters to deal with large power system studies, a two-level three-phase converter is usually utilized. SPWM applied to a three-phase converter works similar to the half-bridge scheme explained in the previous section. Fig.1.12 shows the firing pulse output based con the carrier and the reference signal. The converter is shown Fig.1.10 comprised of 6 switches and each switch with a corresponding firing pulse, denoted as δ_i (i:1-6).

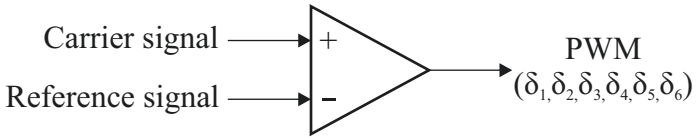

Figure 1.12: SPWM comparator

The reference signal frequency is selected accordingly to the desired voltage output. The carrier signal should be much higher than the reference signal and for this type of converter is around 2000 Hz. Each phase has its own comparator process in which the firing pulses are determined, see Fig. 1.13 . For example, phase A is determined by switches 1 and 4. There are two firing pulses (δ_1 and δ_4) for phase A when one switch is ON, and the other is OFF.

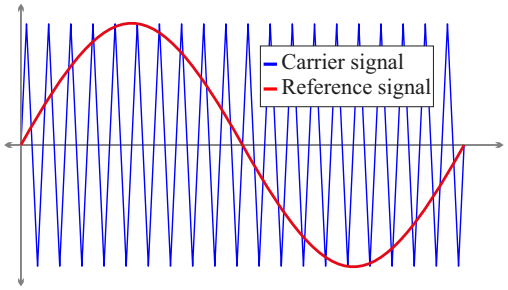

Figure 1.13: SPWM carrier and reference signals

Figure 1.14 shows the firing pulses for δ_1 corresponding to switch S_1 and is generated according to Fig. 1.13. ON or OFF of the switch S_1 depends on the intersection of the carrier and reference signal. When the reference signal intersects with a negative slope, the firing pulse turns ON("1"), and when it has a positive slope the firing pulse turns OFF("0"). Switches S_1 and S_4 are complementary and when one is ON the other must be OFF [37] as shown in Fig.1.14 and Fig. 1.15.

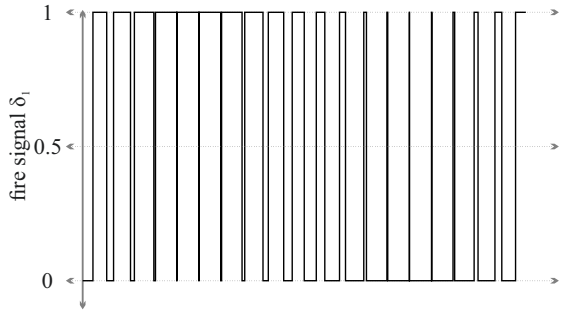

Figure 1.14: Firing pulses δ_1 corresponding to switch 1

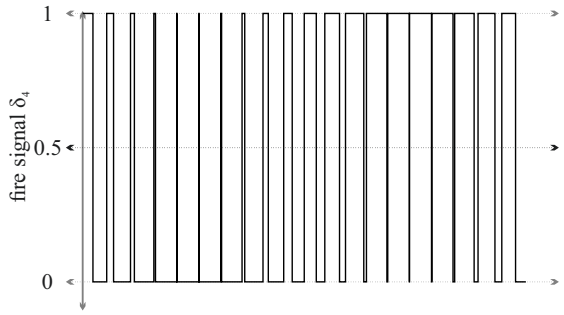

Figure 1.15: Firing pulses δ_4 corresponding to switch 4

1.3 Average and detailed VSC model

VSC requires a high level of computational effort especially if the converter has a multilevel topology, reason why for electrical power system stability studies a average model is usually consider more suitable. The VSC average model utilizes dependent voltage sources on the AC side of the converter and a dependent current source on the DC side as shown in Fig. 1.16. This representation allows the modeling of

several FACTS devices and is widely employed in the modeling of HVDC transmission systems. Although the VSC is a simplified average model, the slow dynamics of the system can be faithfully represented during transient events. As a consequence of that, several studies focused on transient stability can be conducted in large power systems.

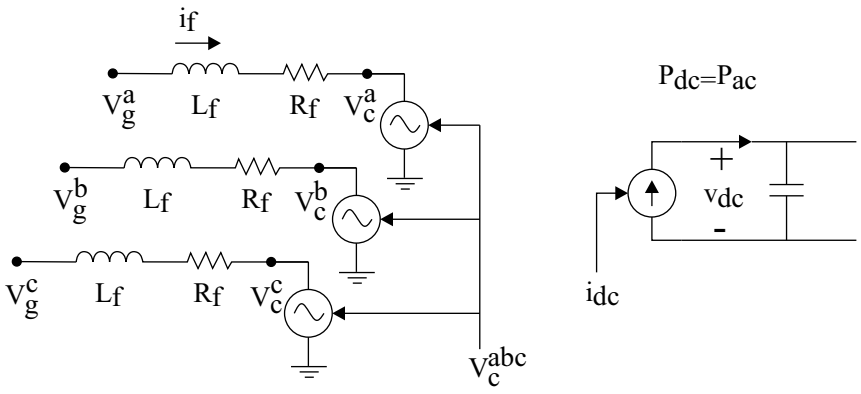

Figure 1.16: Three-phase VSC average model

1.3.1 VSC-HVDC transmission topologies

HVDC transmission systems generally consist of two terminals. In general, there are three types of interconnections: point-to-point, back-to-back, and multiterminal [39]. The use of each will depend on the different performance characteristics, and operational requirements [30]. The point-to-point interconnections have a rectifier and inverter station interconnected by an HVDC transmission line and are classified as follows:

- Monopolar connection: these systems are usually the cheapest and simplest for moderate power transmission since they have only two converters and a high-voltage line of insulated cable or overhead line [3]. Monopolar connections can have their variants: some use the grounded return, others have a metallic return, and others have the midpoint of the 12-pulse converters grounded.

- Homopolar connection: this has two or more DC lines with the same polarity connected to the converters [25]. When a fault occurs in one of the lines, the system will be operating as a homopolar connection. Its high cost has not made it popular, and therefore it is not frequently used [30].

- Bipolar connection: for modern transmission lines, it is the most common configuration together with 12 pulse converters in each terminal [3]. It is similar to the homopolar connection but with different polarities, [30]. Each pole is independent and can operate with a single pole using the ground as return [29].

The HVDC Back-to-Back transmission has the inverter and rectifier station in the same place, which means that the section between them is short and sometimes they are interconnected without a transmission line, directly by buses [19]. This type of connection is mainly employed to connect asynchronous power networks. They are also used to control a certain power flow in meshed networks. In addition, they are useful for intermediate support in AC transmission lines to increase the stability of the electrical network [25]. Multiterminal connection: it has two or more sets of converters operating independently and each converter can operate as an inverter or rectifier [30], [20]. This type of connection is an attractive option to integrate renewable energy systems into the grid such as offshore wind power [26], becuase a HVDC system improves the redundancy of the system, gives greater flexibility in the exchange of power, and reduces initial investment and costs per operation [6]. This technology is one of the newest and with great opportunities for research and development. All described typologies can be seen in Fig. 1.17 and Fig. 1.18

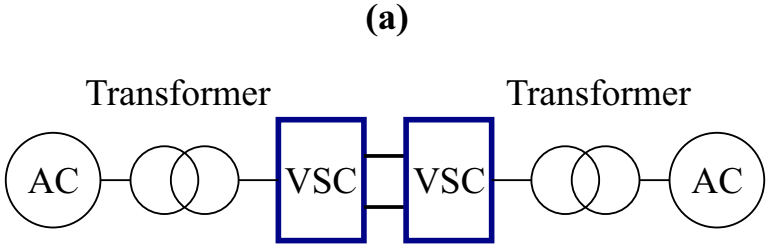

Figure 1.17: Back-to-Back configuration

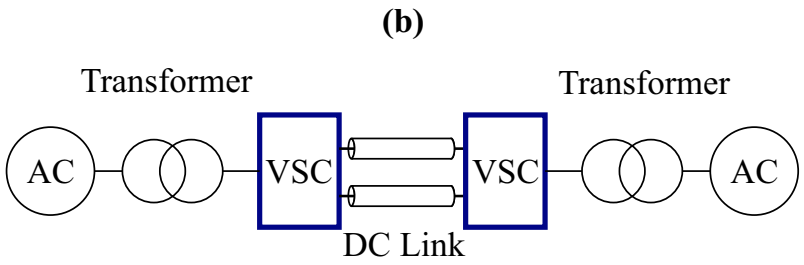

Figure 1.18: Point-to-Point connection that can be either submarine, underground or overhead transmission

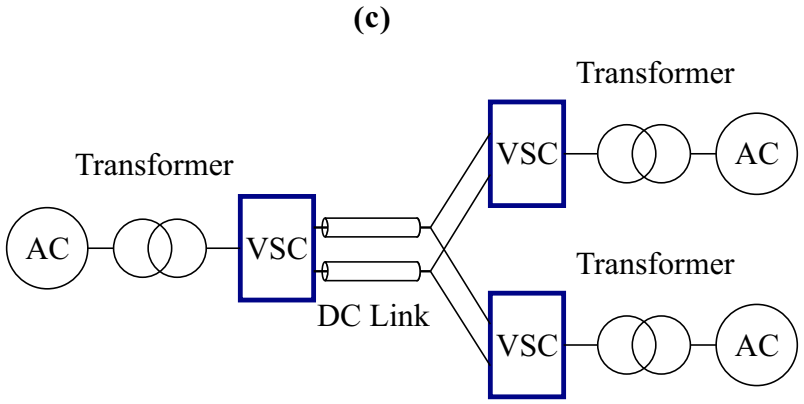

Figure 1.19: Multiterminal connection

1.4 Problem Statement

The continuous growth of electricity demand and the recent integration of renewable energy sources (RES) has created new challenges in the planning, operation, and design of electrical grids to comply with the energetic balance between the generation units and the load centers (end consumers). The expansion of the grid and the increase in electricity consumption have brought the need to develop new power generation projects by considering different energetic resources. Regardless of the generation technology (hydro, coal, nuclear, RES, etc.), the generation plants are increasingly farther away from the cities, this entails the planning of new transmission lines that many times result in long distances. As of matter of fact, the power transmission at long distances has always been studied because there are some essential technical aspects to be considered such as voltage regulation, low short-circuit ratio SCR, high

energy losses, and decreased power stability. These issues should be addressed at aiming to keep an optimal grid operation.

The development of high-power solid-state drives has brought many opportunities for improving grid robustness by addressing the issues mentioned previously. Features like a fast dynamic response of voltage control through reactive power injection, low SCR connection capabilities, and bulk power transmission with fewer active power losses are some of the options offered by these types of devices. Solid-state devices are electronic-based systems and among them, there is a particular type of converter called Voltage Source Converter (VSC). VSC is widely used for several applications such as in High Voltage Direct Current (HVDC) transmission and also in modern power systems that use flexible alternating current transmission systems (FACTS). Even though VSC offers a fast dynamic response, which has a non-linear control system where its tuning and design can be challenging every time a planning or operation issue wants to be evaluated by using dynamic simulations. In this context, this thesis proposes a data-driven control system for VSC, the proposal offers a faster and better dynamic response satisfying a stability criterion. The new controller will be compared to the existing "model-based" controller under several conditions and on three types of VSC devices.

1.5 Objectives

1.5.1 General Objective

Develop a control strategy to enhance the dynamic performance of voltage source converters during transient scenarios coming from transient faults and non-faulted transient events. The aim of this research is based on a control strategy prompted by a data-drive approach.

1.5.2 Particular objectives

This thesis has different particular goals that are listed as follow:

- Modeling of voltage source converters for AC/DC power grids.
- Developing a data-driven-based controller based on the dynamic response of a model-based controller.
- Assessment of a data-driven controller used in STATCOM, BESS, and VSC-HVDC transmission system.
- Comparison of a data-driven model against a model-based controller.

1.6 Methodology

Many approaches have been made recently to improve power system dynamics in presence of electronic-based converters. Some of them use auxiliary control loops to enhance the converter response, and others utilize data-driven control to boost the existing auxiliary control. This opens the possibility of creating a data-driven control for voltage source converter controllers to help improve the dynamic response of the grid by means of offering a fast and robust performance under transient scenarios. In other words, the model-based controller can be entirely replaced by a data-driven controller, specially designed to enhance the dynamic performance of a model-based controller. To this end, a wide variety of dynamics should be addressed aiming to mimic the model-based controller behaviour.

So that, the methodology is divided in three stage; the fist on focuses on creating a data set using a model-based control that allows capturing the dynamic response under several operating conditions by changing the set-points of the input variables. Once the data is acquired, the second stage consists of designing a robust and stable controller. The proposed controller should comply with a particular structure based on theory control. The last one stage, it is to validate the performance of the proposed data-driven controller, which is adressed in multiple devices such as STATCOM, BESS and HVDC transmission systems. Finally, the dynamic performance of the most essential variables is compared to the model-based controller under transient events such as step response changes, load shedding, and three-phase faults.

1.7 Thesis outline

This thesis is organized in four chapter:

- **Chapter 1** contains an overview of HVDC, voltage source converters VSC, Line commutated converters LCC and their applications. It compares the different types of converter, VSC and LCC. The advantage of HVDC transmission compared to AC transmission are discussed. It includes the electric diagram of a VSC station, describes the operation of each part and also shows its sizing. The half-bridge converter basic operation is explained including the pulse-width modulation PWM technique which is fundamental on voltage source converter.

- **Chapter 2** develops the model used for VSC. It starts from the most basic equation such as the Kirchhoff's voltage laws, it also uses the Park's transformation to simplify the control, to finally generate the block diagram to control a VSC. This chapter also describes the different modes of operation of a VSC and explain which is more suitable for every application.

- **Chapter 3** creates a data-driven model based on the dynamic response of the model-based controller presented in the previous chapter.

- **Chapter 4** makes a comparison between the model-based converter and the data-driven converter. Some of the aspects evaluated are voltage step response, voltage recovery under transient faults, and load shedding assessment.

Chapter 2

Modeling of Voltage Source Converters

This chapter presents the modeling of an average VSC used in power system analysis. The dynamic model is simplified using Park's Transformation and an average model is considered to reduce the computational burden. VSC has several applications such as transmission, called VSC-HVDC transmission. It is also used to compensate the reactive power with devices called Static Synchronous Compensators (STATCOMs). When there's energy stored in batteries, a VSC can be used to model Battery Energy Storage System (BESS). In this chapter, the four devices mentioned above are modeled, but the VSC applications are not limited to that number of devices.

2.1 Voltage Source Converters

To deal with large power system studies focused on transient stability or voltage stability, average VSC models have been employed to carry out several studies in power grids depending on the control target. The control design of the converter may vary, and some of the designs are more accurate than others. However, for large power systems an average model is usually used to decrease the computational

complexity [18]. For example, a two-level VSC is usually employed to analyze high-power converters connected to grid. This model represents faithfully the low frequency dynamics of the system, especially for addressing transient stability studies or voltage stability in power grids. For studies other transient phenomena, more detailed models should be employed. To provide an overview of the controller operation, a general scheme is shown on Fig.2.1. The control diagram has multiple steps, starting with the measurements, followed by system variables transformation from *abc* reference frame to another reference frame $dq0$, then a reference is created by multiple outer control loops, finally the inner control provides the outputs.

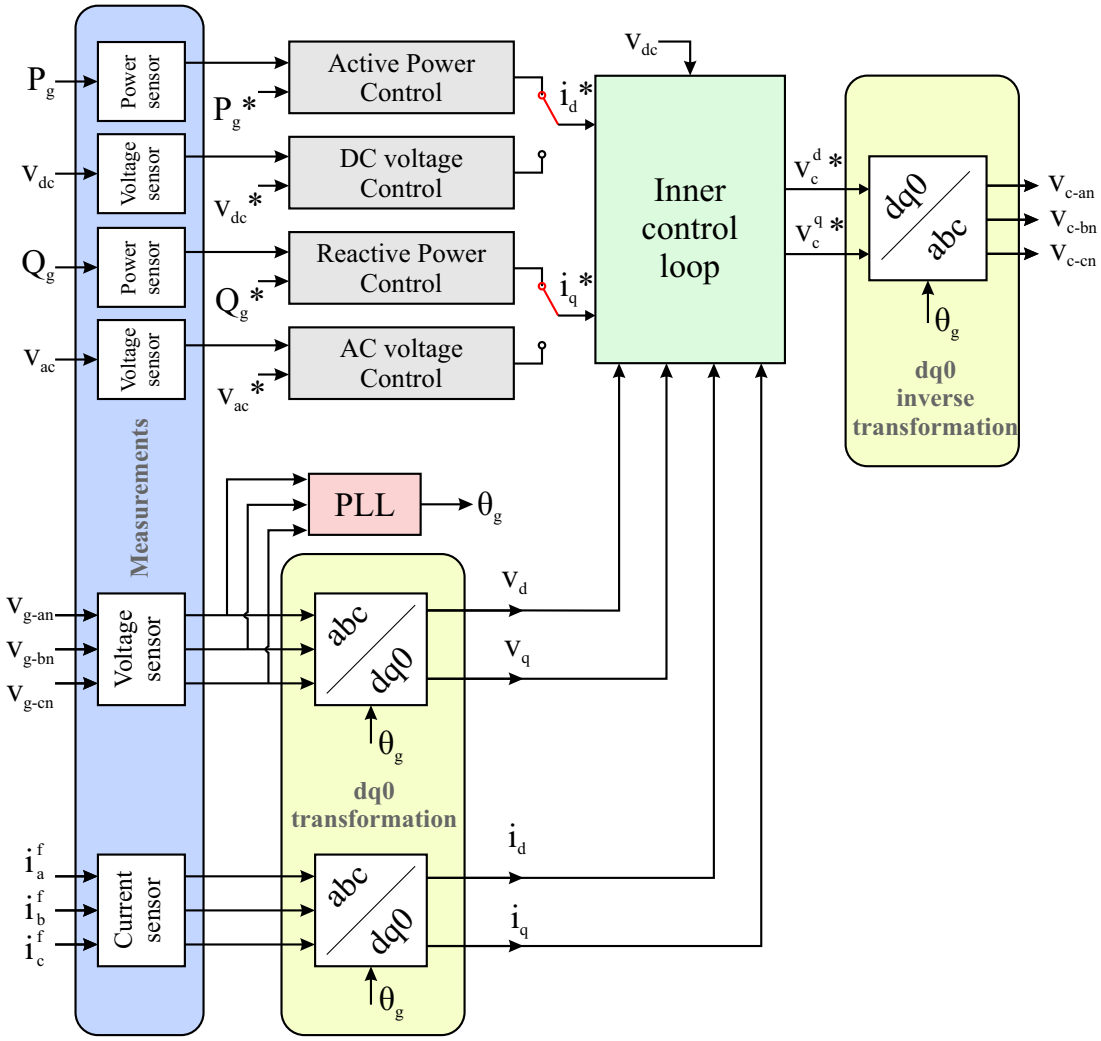

Figure 2.1: Control diagram.

2.1.1 Conventional VSC

An VSC average model is shown in Figure 2.2, which represents a conventional VSC that is modelled by one controlled voltage source on the AC side while the DC side is represented by a controlled current source. The conventional VSC is also referred to as an average model, which is represented in Figure 2.2. This model consists of one controlled voltage source on the AC side and another controlled current source on the direct current (DC) side.

The state-space model of the conventional VSC converter is derived by the connection to the grid through a power transformer; therefore, its control can be performed by the impedance Z_f among two buses v_g and v_c, defined by L_f and R_f. The equivalent circuit of the grid is represented by a grid impedance Z_s and a voltage source V_s.

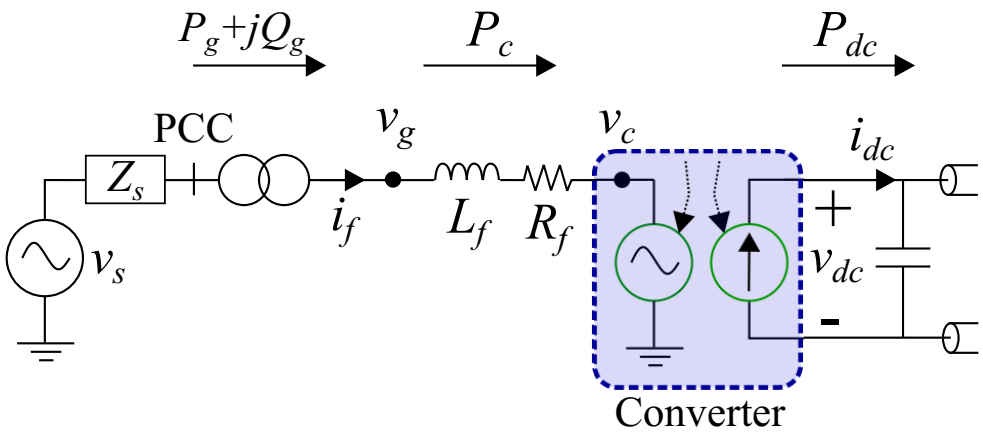

Figure 2.2: Average VSC model.

According to Figure 2.2 and considering the Kirchhoff's voltage law in the *abc* reference frame, the voltage drop along the impedance Z_s is:

$$v_g^{abc} - v_c^{abc} = L_f \frac{di_f^{abc}}{dt} + R_f i_f^{abc}. \tag{2.1}$$

Applying Park's Transformation $dq0$ and considering ω_g as the angular frequency of the rotating system; Equation (2.1) can be rewritten by dividing the real and

imaginary parts, giving the next expressions as a result [21]:

$$L_f \frac{di_f^d}{dt} = \omega_g L_f i_f^q - R_f i_f^d + v_g^d - v_c^d, \tag{2.2}$$

$$L_f \frac{di_f^q}{dt} = \omega_g L_f i_f^d - R_f i_f^q + v_g^q - v_c^q. \tag{2.3}$$

Equations (2.2) and (2.3) define the $dq0$-rotating frame where the q-component tends to be zero in steady-state [17]. This means that, the $dq0$-rotating frame must be synchronized with the abc-reference frame via a Phase-Locked Loop (PLL). For controlling purposes, active and reactive powers need to be expressed in the $dq0$-rotating frame as:

$$P_g = v_g^d i_f^d \tag{2.4}$$

$$Q_g = -v_g^d i_f^q. \tag{2.5}$$

The controlling purpose of a VSC is to offer an independently control into the active power P (or DC voltage) and reactive power Q (or AC voltage) according to the reference point [42]. To this end, two controllers are used, an outer-control loop and an inner-control loop. Both controllers are derived from the mathematical equations developed previously. The outer-control loop calculates the reference signals for i_f^{d*} and i_f^{q*}, which are employed as inputs to the inner-control loop. The inner-control loop gives the reference voltage [21] to V_c (controlled voltage source). Depending on the target of control, the VSC can work either as a rectifier or inverter. Considering a lossless converter, the power balance equation in the $dq0$ reference frame is [38]:

$$P_{dc} = P_{ac} = v_{dc} i_{dc} = v_g^d i_f^d + v_g^q i_f^q. \tag{2.6}$$

Expression (2.6) can also be rewritten as:

$$i_{dc} = \frac{v_g^d i_f^d + v_g^q i_f^q}{v_{cd}}. \tag{2.7}$$

In this case, Equation (2.7) provides the input signal to the controlled current source on the DC side of the VSC.

2.1.2 Model-Based Control

The control loops of a VSC-based STATCOM model are defined by a model-based control; basically, the first controller corresponds to the outer loop depending on the variable to be controlled, V_{dc} (or P) and V_{ac} (or Q_ac). The second controller represents the inner loop according to the state-space model, which is also defined by expressions (2.2) and (2.3). In this way, the conventional control uses a PI-controller, so that, the inner-control loop can be represented as:

$$v_c^d = \omega_g L_f i_f^q - \left(K_p - \frac{K_i}{s}\right)\left(i_f^{d*} - i_f^d\right) + v_g^d \tag{2.8}$$

$$v_c^q = -\omega_g L_f i_f^d - \left(K_p - \frac{K_i}{s}\right)\left(i_f^{q*} - i_f^q\right) + v_g^q. \tag{2.9}$$

Additional details about the model-based controller can be found in [23].

2.1.3 Control loops

The control block diagram of the VSC consists basically of two control loops: the outer control loop and the inner control loop. Both are derived from the mathematical equations developed previously. The VSC is capable of controlling independently active power P, DC voltage on the rectifier side, and reactive power Q and ac voltage on the inverter side [18]. By controlling i_f^d and i_f^q in Equation 2.4 and Equation 2.5

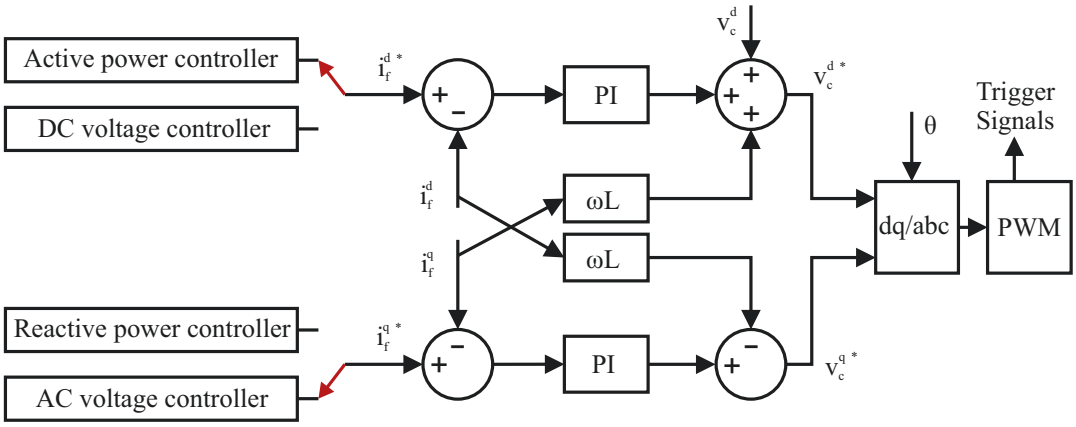

Figure 2.3: VSC block control diagram.

the inputs and outputs of the VSC link can be manipulated. The converter control consists of a two-stage control of two cascaded PI-controller[18]. Where the PI can be represented as[18]:

$$K(s) = K_p + \frac{K_i}{s} \tag{2.10}$$

where K_p and K_i are the proportional gain and integral gain, respectively.

Active power controller

The active power controller creates a reference for i_f^{d*}. The active power reference is set by the user and the measured power is taken from V_g and i_f. A PI controller is used, and the output goes into the inner control loop. The proportional and integral gains depend on the system impedance and not on the phase reactor, which makes its tunning more difficult.

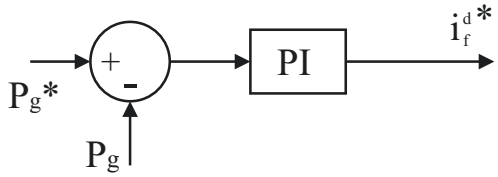

Figure 2.4: Active power block control diagram.

Reactive power controller

The reactive power controller creates a reference for $i_f^{q^*}$. It is usually used both the rectifier side and the inverter station. Like any other outer controller, the proportional and integral gains depend on the power system impedance.

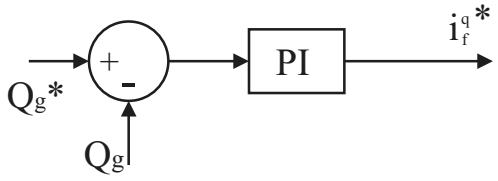

Figure 2.5: Reactive power block control diagram.

AC Voltage controller

The AC voltage controller establishes a reference signal for $i_f^{q^*}$. The measured magnitude of V_g is compared to the reference defined by the user. The AC controller is usually used in the inverter side to support the AC voltage of the grid.

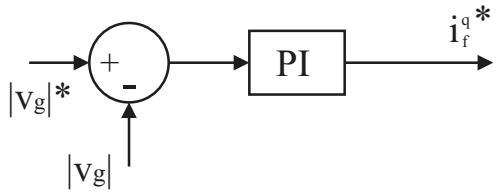

Figure 2.6: AC voltage block control diagram.

DC Voltage controller

The DC controller aims to create a reference for $i_f^{d^*}$. This is useful when the DC voltage variable needs to be controlled due to any STATCOM requires a constant DC voltage in order to work properly.

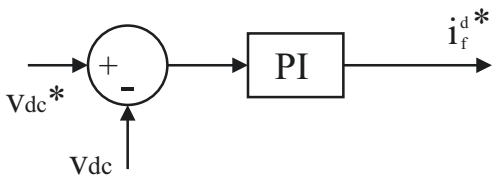

Figure 2.7: DC voltage block control diagram.

2.1.4 Phase-Locked Loop (PLL)

The PLL is of utmost importance when modeling a VSC. PLL tracks the grid phase and frequency[15] aiming to synchronize the VSC output voltage with the grid voltage. The phase helps change from *abc* reference frame to *dq*0 reference frame and vice versa. That is, the voltages and currents of a *abc* reference frame are transformed to a *dq0* reference frame.

PLL can be considered a servo system and it is comprised of three main building blocks: Phase Detector, VCO (Voltage Controlled Oscillator), and Loop filter[35] as shown in Fig.2.8. The main target of a PLL entails the tracking of a signal compared to a generated reference signal [15]. The Phase Detector measures the input phase, which compares it with the reference, and sends an error signal proportional to the phase difference. VCO receives the error signal from the Phase Detector and tries making the error zero producing the output frequency equal to the input frequency [35]. The low-pass filter eliminated the noise and high-frequency signal component from the Phase Detector[15].

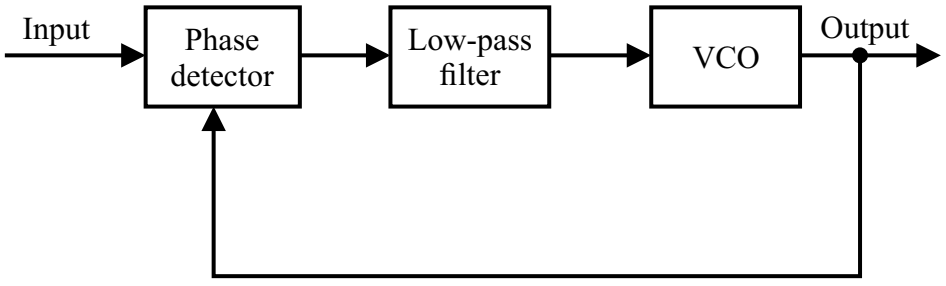

Figure 2.8: PLL basic structure

2.1.5 PQ Capability

The power capability of VSC can be particularized using a PQ capability diagram as shown in Fig. 2.9. The regions of operation of VSC depend on its role in the power system. When reactive power is supplied by the converter the region of operation is positive reactive power and when the reactive power is negative, it means reactive power is being absorbed by the converter. STATCOM, BESS, and VSC-HVDC have different modes of operation. For example, STATCOMs to keep a reference voltage must supply reactive power and the real power transfer (absorbed/supplied) must be close to zero.

The maximum apparent power is limited by the circle and the reactive power limit is represented by the purple region. The reactive power limits are usually defined by the AC terminal voltage[18].

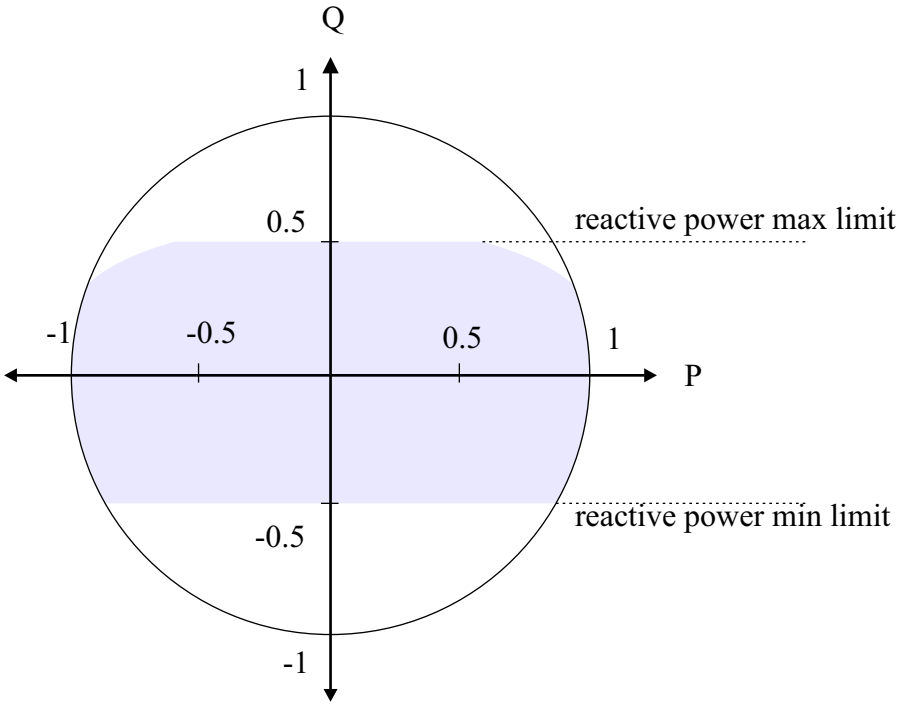

Figure 2.9: PQ capability [18]

2.1.6 VSC-HVDC Operation

A VSC-HVDC transmission system is usually comprised of three elements: AC part, DC part, and the converting stations (VSC). The basic configuration is represented in Figure 2.10. The two AC networks can be independent of each other (i.e. different frequency, phase, etc.) and the DC link establishes a flexible bound between one another.

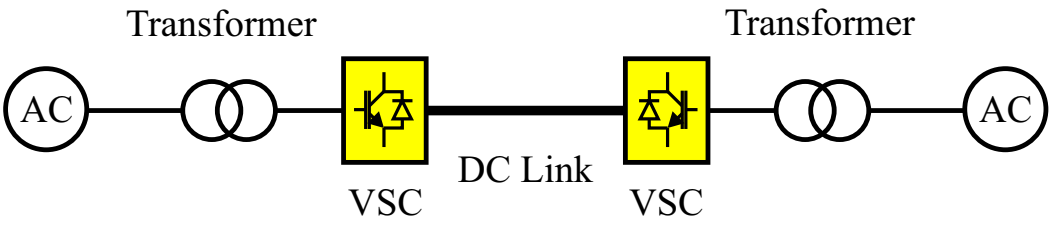

Figure 2.10: Single line diagram of a VSC-HVDC transmission system

The VSC-HVDC works as a controllable voltage source with enables the possibility to control active and reactive power independently, a feature, that's not possible to achieve using LCC-HVDC technology in which the active and reactive power is subjected to the firing angle of the thyristors.

$$FP = \cos\phi = \cos\alpha \tag{2.11}$$

where α is the firing angle of the thyristor, ϕ is the complex power angle, and FP represents the power factor [22].

VSC offers the possibility to perform power reversal between each converter station without having to change polarity [36]. The DC link must maintain a fairly DC voltage, which at the same time can be controlled by one of the stations. One of VSC-HVDC stations operates as a rectifier and the other as an inverter. The rectifier usually is set to control AC terminal voltage and active power. The inverter controls the DC voltage (DC side) and AC terminal voltage. Controlling reactive power in any side of the VSC-HVDC is not recommend because the amount of reactive power injected must be subjected to a voltage profile and also because controlling the AC

terminal voltage improves the system stability. For large power system studies, a two-level average VSC model is usually employed. The use of average models helps reducing the computational burden, this is possible by using dependent voltage source instead of employing the IGBTs switching.

2.1.7 Static Synchronous Compensator (STATCOM) Operation

STATCOMs VSC-based have a similar scheme and control system as the VSC-HVDC but only operate with one converter. STATCOMs are used to control AC terminal voltage by injecting reactive power according to Fig. 2.9. The active power transfer must be close to null and the DC voltage should be controlled so that there is a proper operation of the device. In this case, the VSC is used as a static VAR generator that can operate as an inductive or capacitive device. Since the real power transfer, P_c between the grid and converter are equal considering a lossless system (neglecting energy loss in the semiconductor switches) must be zero which means that v_g and v_c must have the same phase as shown in Eq. 2.12.

$$P_c = \frac{v_g v_c}{x_f} \sin(\theta_g - \theta_c) = 0 \tag{2.12}$$

$$\sin(\theta_g - \theta_c) = 0 \tag{2.13}$$

$$\theta_g - \theta_c = 0 \tag{2.14}$$

$$\theta_g = \theta_c \tag{2.15}$$

The reactive power at zero frequency on the DC side is zero, meaning that the capacitor on the DC side plays no role in the reactive power generation[12].

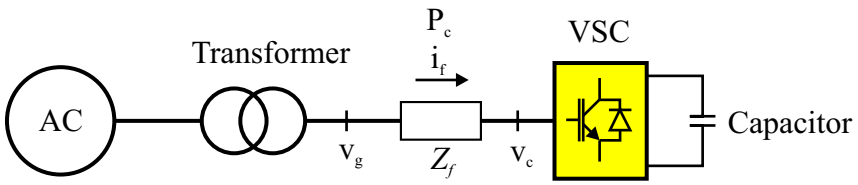

Figure 2.11: Basic STATCOM connection to the grid

2.1.8 Battery Energy Storage Systems Operation

The continuous integration of RES into conventional power grid creates power generation uncertainties[8]. RES power generation dispatch cannot be control and depend entirely on nature conditions, this aspect creates an unbalance condition between the amount of power that is produced versus that which is consumed leading to stability issues. In theory, the generation variation due to the nature of the RES is compensated by another type of source that is capable of delivering power fast, such as hydroelectric, but currently other ways are being explored to avoid this problem like energy storage devices such as Battery Energy Storage Systems BESS.

Chapter 3

Data-Driven Control

In this section, the fundamentals that constitute the basis of data-driven controllers are introduced.

3.0.1 General Notation

- $\mathbb{R}$ represents the set of reals
- $\mathbb{Z}_+$ corresponds to the set of positive integers.
- $\mathbb{R}^q$ is real vectors of dimension q.
- $\mathbb{R}^{p\times q}$ stands for real matrices of dimension $p \times q$.
- I_q denotes an identity matrix with q rows and q columns.
- $\text{col}(x_1, x_2)$ is a vector obtained after stacking column vectors x_1 over x_2.
- $\text{rank}(M)$ represents the rank of matrix $M \in \mathbb{R}^{p\times q}$.
- $\text{colspan}(M)$ is the set of all linear combinations of its column vectors.
- σ denotes the shift operator, which applies to a function $f : \mathbb{Z}_+ \to \mathbb{R}^q$ in the form $(\sigma f)(t) := f(t + 1)$.

– $(\sigma^N f)(t) := f(t+N)$ is an operator extended to an order N.

3.0.2 Data-driven Control Overview

The develop of a data-driven controller, several steps are taken into account. Figure 3.1 presents an general overview of the controller design process, which has multiple steps and properties to comply with the desired characteristics such as stability criteria, sufficiency of information, etc.. To deal with the development of the controller prompted by data-driven, we can start by gathering measurements that disclose the system dynamics for different operating points. The data is used as input to the control design which is based on the measured variables (time-discrete data). The control design follows many particular criteria defined by the control theory and can be solved by an optimization approach in order to comply with the stability function. After that, the new control approach has to be tested to analyse its performance.

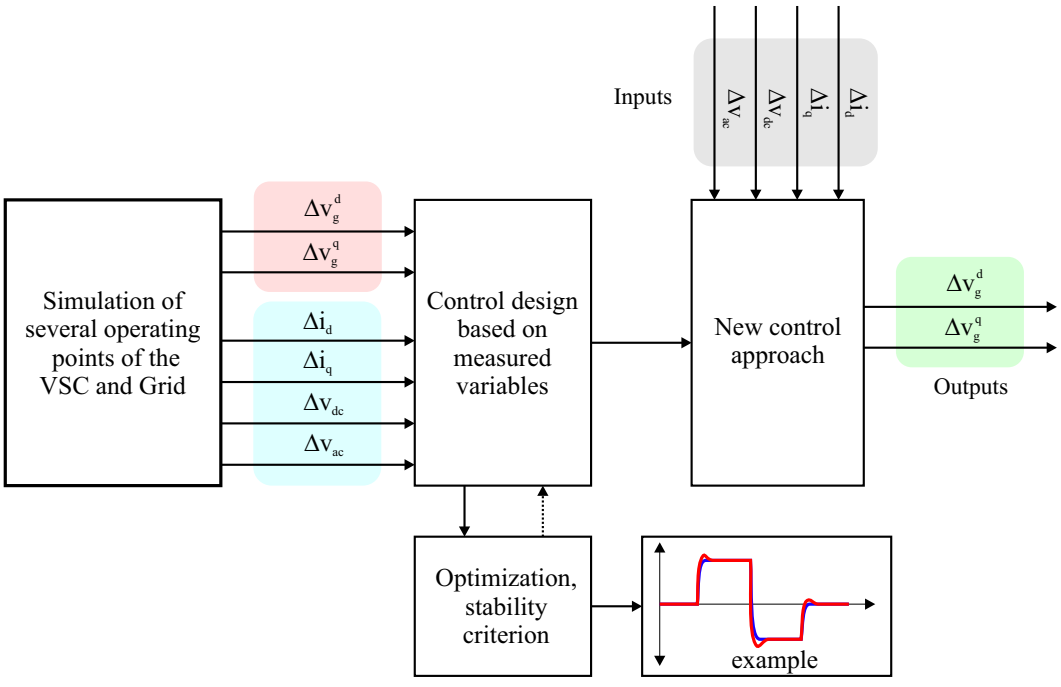

Figure 3.1: Data-driven general process diagram

3.0.3 Linear Difference Systems

To study discrete-time linear systems, one can use linear difference equations that can be represented by their general form:

$$R_0 w + R_1(\sigma w) + \cdots + R_N(\sigma^N w) = 0, \tag{3.1}$$

where the discrete time function $w : \mathbb{Z}_+ \to \mathbb{R}^q$ maps time instants into physical amounts or measurements of electrical variables; the maximum degree of the shift operator σ is represented by N; and $R_i \in \mathbb{R}^{p\times q}$ $(i = 0,\ 1, ...,\ N)$.

The expression (3.1) can be expressed employing a compactly form as:

$$R(\sigma)w = 0\ ; \tag{3.2}$$

where $R(\sigma)$ is a $p \times q$ polynomial matrix in σ, and represents the physical laws of the system with respect to w.

The components of w are classified as either inputs or outputs, where the input functions are denoted by u, which are independent (v.g., control variables). The output functions are results due to the inputs (v.g., state variables), and are denoted by y. These variables can be organized as an *input/output partition*, that is, $w := \mathrm{col}(u, y)$.

3.0.4 Quadratic Difference Forms (QdFs)

Lyapunov functions have been widely used to study the stability of systems, and other important properties of linear difference systems. In this work, the notion of quadratic difference forms (QdFs), which are functionals of the discrete-time function

w and its time-shifts, that is,

$$Q_\Psi(w) = \begin{bmatrix} w^\top & \sigma w^\top & \cdots & \sigma^N w^\top \end{bmatrix} \widetilde{\Psi} \begin{bmatrix} w \\ \sigma w \\ \vdots \\ \sigma^N w \end{bmatrix} , \tag{3.3}$$

where $\widetilde{\Psi} \in \mathbb{R}^{Nq \times Nq}$ is referred to as the coefficient matrix of Q_Ψ. The rate of change of the functional Q_Ψ, denoted as ∇Q_Ψ (an analogous to a continuous-time derivative), is given by

$$\nabla Q_\Psi(w)(t) := \sigma Q_\Psi(w)(t) - Q_\Psi(w)(t) . \tag{3.4}$$

Stability of any autonomous system can be studied through QdFs. A system will be autonomous if the polynomial matrix $R(\sigma)$ in (3.2) is square and nonsingular (see [40]). An autonomous linear difference system is asymptotically stable if

$$\lim_{t \to \infty} w(t) = 0 , \quad \forall \ w \quad \text{satisfying (3.2).}$$

According to the Lyapunov approach, the system defined by (3.2) will be is asymptotically stable if a QdF Q_Ψ exists and is such that, $\forall w$ satisfying (3.2), the following holds:

$$\text{(i)} \ \ Q_\Psi(w) \geq 0, \text{ and}$$

$$\text{(ii)} \ \ \nabla Q_\Psi(w) < 0.$$

Finally, the QdF Q_Ψ that satisfies the above inequalities is referred to as the *Lyapunov function.*

3.0.5 Stabilization

The design of a controller not only should regulate the system variables to a predefined set-point but also guarantee stability during disturbances that typical occur in an

electrical system. In terms of linear difference systems, the equations of the plant and the controller can be represented as in (3.2), that is, by $P(\sigma)w = 0$ and $C(\sigma)w = 0$, respectively. Besides, the interconnected (closed-loop) system can be represented by:

$$\underbrace{\begin{bmatrix} P(\sigma) \\ C(\sigma) \end{bmatrix}}_{R(\sigma)} w = 0 \,, \tag{3.5}$$

where the laws of plant $P(\sigma)w = 0$ and controller $C(\sigma)w = 0$ must be simultaneously satisfied by w. This means that, by choosing a suitable controller, the trajectories of the system can be restricted to those that are asymptotically stable and discard those that are undesirable; for example, unstable, highly oscillatory, too slow, and so forth.

The design of controller $C(\sigma)$ can impose the stability on (3.5). For this, it must be guaranteed that, having a partition $w = \mathrm{col}(u, y)$, the stability conditions recalled in Section 3.0.4 for a Lyapunov function candidate Q_Ψ, hold for all w satisfying (3.5). Notice that, if the coefficient matrix satisfies $\widetilde{\Psi} > 0$, then $Q_\Psi \geq 0$ prevails. Hence, it is still necessary to guarantee that $\nabla Q_\Psi < 0 \ \forall w$ satisfying (3.5). For this purpose, the description of the closed-loop system can be introduced in the inequality, by considering a polynomial matrix $V(\sigma)$, which is non zero, and has the same dimensions as $R(\sigma)$ in (3.5). In this form, the symmetry necessary to satisfy the inequality is preserved, that is,

$$\underbrace{\sigma Q_\Psi(w) - Q_\Psi(w)}_{\nabla Q_\Psi(w)} + \underbrace{w^\top V(\sigma)^\top \begin{bmatrix} P(\sigma) \\ C(\sigma) \end{bmatrix} w + w^\top \begin{bmatrix} P(\sigma) \\ C(\sigma) \end{bmatrix}^\top V(\sigma) w}_{\text{Symmetric component}} < 0 \,. \tag{3.6}$$

Notice that the condition imposed by inequality (3.6) is interpreted as follows: if a QdF $Q_\Psi \geq 0$ (i.e., $\widetilde{\Psi} > 0$) exists and is such that (3.6) is satisfied, then the asymptotic stability is guaranteed for the interconnected system (3.5). This follows from the fact that every trajectory w satisfying the interconnected system laws, will cancel out the additional symmetric component (because $P(\sigma)w = C(\sigma)w = 0$), which meets

the condition $\nabla Q_\Psi < 0$, concerning the trajectories w produced by the closed-loop system (3.5).

In order to generate a numerical solution to this algebraically complex condition, it is proposed to use a candidate controller computed by the available measurement data whose gains are unknown, rather than a model of the system. This entails that the plant mathematical model will be ultimately substituted by a condition on coefficient matrices built entirely from data.

3.1 Bypassing Models Using Data

The control design is carried out by employing data that not only takes into account the converter dynamics but also the power systems dynamics caused by transient events. This enables the possibility to synthesize controllers wholly from data of available measurements leading to a simplified route for the classic system identification (modeling and parametric identification) plus a model-based control approach. This is illustrated in Figure 3.2, where one can observe two ways of implementing controller; in this context, the main contribution of this work is entirely focused on the design of controllers following the fundamentals of data-driven control.

Moreover, both stability conditions and the desired performance must be completely comparable with a model-based scheme. This is also fully related to the basic empiric gain-tuning rules for classic P, PI, and PID controllers, which do not require a model of the system, but cannot guarantee stability and performance in a deterministic way (see [14, 9]). Therefore, the controller of a VSC should be purely designed from measurements that permits to omit the need of an explicit mathematical model without losing stability and general performance capabilities with respect to a model-based technique.

The design process begins employing essential conditions to assure that the available measurements (measured data) are convenient for control design. As a con-

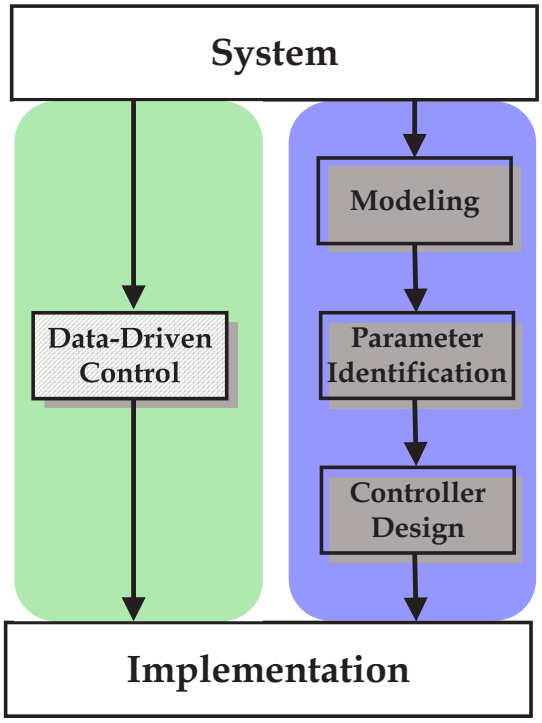

Figure 3.2: Proposed data-driven control vs. traditional "system identification + model-based" approach.

sequence of that, this work introduces a general test that determines whether the information provided by the available data is sufficient to fully recuperate the system physical laws, which is described in the next subsection.

3.1.1 Information Sufficiency

All electrical quantities are sampled signals according to a sampling rate. In fact, all measurements w are stored in a vector of data $\{w(1), w(2), ..., w(T)\}$ of length T. Associated with this set of measurements, a *Hankel matrix* with a depth of $L < T \in \mathbb{Z}_+$ can be expressed as follows:

$$\mathcal{H}_L(w) := \begin{bmatrix} w(t) & \sigma w(t) & \cdots & \sigma^{(T-L+1)}w(t) \\ \sigma w(t) & \sigma^2 w(t) & \cdots & \sigma^{(T-L+2)}w(t) \\ \vdots & \vdots & \cdots & \vdots \\ \sigma^L w(t) & \sigma^{(L+1)}w(t) & \cdots & \sigma^T w(t) \end{bmatrix}. \tag{3.7}$$

According to the expression (3.7), notice that σ denotes the shift operator, that is, samples at different time instants for discrete systems. In this sense, to verify the sufficiency of information, the available data must be sufficient to take back the system's physical laws, and the persistency of excitation concept [41] is employed. This is a condition that applies for the input functions u in $w = \text{col}(u, y)$, which is defined as follows. A vector $u = u(1), u(2), ..., u(T)$ of order L is said to be persistently exciting (PE) if matrix $\mathcal{H}_L(u)$ has full row rank.

Assuming that u is PE of at least order L, where L equals the sum of the number of inputs plus the state-space dimension (see Theorem 1 in [41]); out of this, colspan($\mathcal{H}_L(w)$) represents the set of all possible solutions of (3.2). That is, if the input is PE, then the complete dynamics of the electrical system can be fully described by the set of the available measurements. While a model is able to determine all the possible outcomes of an electrical system as the solution of linear difference or differential equations; similarly, one can do the same by taking into consideration the linear combination of the row vectors of the Hankel matrix $\mathcal{H}_L$. Consequently, this array of data in a matrix owns the same model information.

3.1.2 Data-Based Coefficient Matrices

In this section we show the connection between matrices constructed from data and the models studied in subsections (3.0.3) and (3.0.4). Based on (3.1) and taking into

account the above kernel representation (3.2), the following factorization is obtained:

$$\underbrace{\begin{bmatrix} P_0 & P_1 & \cdots & P_N \end{bmatrix}}_{\widetilde{P}} \begin{bmatrix} w \\ \sigma w \\ \vdots \\ \sigma^N w \end{bmatrix} = 0 \, ; \tag{3.8}$$

where $\widetilde{P}$ (a block matrix) is referred to as the coefficient matrix. It is shown next that this matrix can be directly obtained out of measured data. For this purpose, consider expression (3.7) for $L = N + 1$, w with sufficiency of information and N representing the maximum degree of the shift operator.

After organizing all measured data, which are stored in $\mathcal{H}_{N+1}$, it is appealed to the singular-value decomposition (SVD) which is defined as:

$$\mathcal{H}_{N+1}(w) := U \Sigma V^{\top} \tag{3.9}$$

where matrices U and V are square $(q \times q)$ and orthogonal; Σ represents a diagonal matrix having non-negative real numbers on its diagonal, which are referred to as singular values.

Furthermore, there is a number given by $r := \operatorname{rank}(\mathcal{H}_{N+1}(w))$ that accounts for non-zero singular values. It can be demonstrated, out of the last $(q-r)$ rows of zeros of $U^{\top} H(w)$, that $U^{\top}$ has annihilators of w (i.e., the set of vectors $\mathcal{V}$ such that $\mathcal{V} w = 0$). Hence, after analyzing the partition $U := \begin{bmatrix} U_1 & U_2 \end{bmatrix}$, where U_1 owns r columns, the left kernel $\widetilde{P} := U_2^{\top}$ can be retrieved. Notice that matrix $U_2^{\top}$, built entirely from measurement data, owns the same information as that offered by the coefficient matrix $\widetilde{P}$, which is derived from an explicit mathematical model. Based on this proven equivalence, it is possible to get around the need for an explicit mathematical model representation and to directly design controllers considering only measured data and assisted by numerical tools.

3.2 Data-Based (Model-Free) Control

This section focuses on designing controllers emanate from measured data. The methodology employs the calculation of linear matrix inequalities (LMIs). For this, let us consider that the elements of (3.6) can be factored in terms of coefficient matrices as described next. Notice that the energy rate of change can be factored as follows:

$$\nabla Q_{\Psi}(w) = \underbrace{\begin{bmatrix} w \\ \sigma w \\ \vdots \\ \sigma^N w \end{bmatrix}^{\top} \begin{bmatrix} 0_{q\times q} & 0_{q\times Nq} \\ 0_{Nq\times q} & \widetilde{\Psi} \end{bmatrix} \begin{bmatrix} w \\ \sigma w \\ \vdots \\ \sigma^N w \end{bmatrix}}_{\sigma Q_{\Psi}(w)} - \underbrace{\begin{bmatrix} w \\ \sigma w \\ \vdots \\ \sigma^N w \end{bmatrix}^{\top} \begin{bmatrix} \widetilde{\Psi} & 0_{Nq\times q} \\ 0_{q\times Nq} & 0_{q\times q} \end{bmatrix} \begin{bmatrix} w \\ \sigma w \\ \vdots \\ \sigma^N w \end{bmatrix}}_{Q_{\Psi}(w)} . \tag{3.10}$$

Based on the coefficient matrix definition for the plant dynamics presented in (3.8), and defining coefficient matrices for $C(\sigma)$ and $V(\sigma)$, the following factorizations can be obtained

$$\begin{bmatrix} P(\sigma) \\ C(\sigma) \end{bmatrix} w = \begin{bmatrix} \widetilde{P} \\ \widetilde{C} \end{bmatrix} \begin{bmatrix} w \\ \sigma w \\ \vdots \\ \sigma^N w \end{bmatrix} , \quad V(\sigma)w = \widetilde{V} \begin{bmatrix} w \\ \sigma w \\ \vdots \\ \sigma^N w \end{bmatrix} . \tag{3.11}$$

Notice that, out of factorizations (3.10)–(3.11), condition (3.6) can be entirely written in terms of coefficient matrices, that is,

$$\begin{bmatrix} 0_{q\times q} & 0_{q\times Nq} \\ 0_{Nq\times q} & \widetilde{\Psi} \end{bmatrix} + \begin{bmatrix} \widetilde{\Psi} & 0_{Nq\times q} \\ 0_{q\times Nq} & 0_{q\times q} \end{bmatrix} + \widetilde{V}^{\top} \begin{bmatrix} \widetilde{P} \\ \widetilde{C} \end{bmatrix} + \begin{bmatrix} \widetilde{P}^{\top} & \widetilde{C}^{\top} \end{bmatrix} \widetilde{V} \geq 0 \, ; \tag{3.12}$$

Consequently, if there is a $\widetilde{\Psi} = \widetilde{\Psi}^{\top} \geq 0$, $\widetilde{X} \in \mathbb{R}^{(N+1)q\times(N+1)q}$ and $\widetilde{C} \in \mathbb{R}^{(q-m)\times(N+1)q}$ such that (3.12) is kept valid, then stability is guaranteed for a plant whose coefficient

matrix $\widetilde{P} \in \mathbb{R}^{(q-m)\times(N+1)q}$ is built upon data. It is noteworthy that the numerical solution of the inequality (3.12) can be solved by conventional MATLAB toolboxes such as `Yalmip`. Therefore, based solely on measurement data to generate $\widetilde{P}$, the coefficients of a stabilizing controller can be obtained without the need for an explicit mathematical model. In other words, the controller given by $C(\sigma)w = 0$ can be realized out of the numerical solution of $\widetilde{C}$ in (3.12).

3.2.1 Candidate Controller for Stabilization

After examining (3.12), one can conclude that there are several solutions that will deliver convenient stabilization controllers for a certain plant. However, regarding electric power systems, there might be a particular interest in finding solutions that exhibit particular requirements, for instance, the regulation of certain variables despite of disturbances. As an example, in this work, a general convenient controller structure is proposed. The associated gains can be implicit in $\widetilde{C}$, and thus they can be numerically calculated after solving (3.12).

The controller design process starts by considering the error variables $\Delta x := x - x^*$, where x represents the original discrete-time function, while x^* is the reference at the equilibrium point (set point). Next, the following proportional feedback current control is proposed:

$$\Delta u := -K\Delta y \,, \tag{3.13}$$

where $\Delta u := u - u^*$ and $\Delta y := y - y^*$ are the error variables of the input u and the output y, respectively. We will denote the number of inputs as l and number of outputs as m; consequently $K \in \mathbb{R}^{m\times l}$.

This control loop can guarantee stabilization by a proper computation of K. Moreover, to ensure the steady-state error compensation, one can add a discrete-time

integrator:

$$\Delta u = -K\Delta y - Gz \; ; \quad \sigma z = z + \Delta y \; ; \tag{3.14}$$

where z corresponds to an auxiliary state-variable to describe the discrete-time integrator of the output variable error, then $G \in \mathbb{R}^{m\times l}$.

By considering $w := \text{col}(\Delta u, \Delta y, z)$ and taking into account (3.13)–(3.14), it is possible to obtain the following representation for the controller:

$$\underbrace{\begin{bmatrix} I_m & K & G \\ 0_{m\times l} & -I_l & \sigma I_m - I_m \end{bmatrix}}_{C(\sigma)} \begin{bmatrix} \Delta u \\ \Delta y \\ z \end{bmatrix} = 0 \; . \tag{3.15}$$

Then, the coefficient matrix $\widetilde{C}$ is described by:

$$\widetilde{C} = \begin{bmatrix} I_m & K & G & 0_{m\times m} & 0_{m\times l} & 0_{m\times l} \\ 0_{l\times m} & -I_l & -I_l & 0_{l\times m} & -I_l & \sigma I_l \end{bmatrix} . \tag{3.16}$$

Now the gains in K and G can be numerically computed as a solution of (3.12) with $\widetilde{P}$ the coefficient matrix of the plant, which is obtained out of measured data w, as explained in Section 3.1.2.

3.3 VSC Using Data-Driven Controller

Data-driven controllers enable a faster dynamic response and these can be applied to VSC. For instance, a VSC-based STATCOM model has been used in the past, where a data-driven approach is studied focusing on an auxiliary control and not to the converter itself [43, 28].

The data-driven controller of VSC is based on the response of the conventional VSC model, and depending on the control requirements, the VSC must be able to

offer faster dynamic response aiming at providing voltage support due to external events such as faults or connection/disconnection of loads.

The data-driven controller consists only of inputs and outputs data and avoids the use of complex mathematical algorithms, which makes it suitable for a large power system that usually requires a high computational burden. The proposed data-driven strategy that is discussed in a general way in Section 3.2, is now described in terms of the VSC variables for its implementation in STATCOM, BESS, and HVDC link.

To set-up the controller, it is not required to know any information about the models of the VSC and the grid. The only requirement is the definition of available variables for control and measurement, as well as an operating point predefined, that is, a set-point. The available variables are accommodated in a vector w, and the set-point of the external variables at the equilibrium is denoted by w^*. Then error variables are denoted by $\Delta w = w - w^*$. Then a set of measurements containing $w(1), w(2), ..., w(T)$ can be used to generate $\Delta w(1), \Delta w(2), ..., \Delta w(T)$, simply by subtracting the operating point value.

In this work, Δi_d, Δi_q, Δv_{dc}, Δv_{ac}, and Δv_c^d, Δv_c^q are selected as the external variables, since they are typically available measurements in practice. Moreover, the variables Δv_c^d, Δv_c^q will permit implementation of the controller, as they provide the voltage reference for the VSC in terms of the dq reference frame.

As described in Section 3.1.1, the collection of data on these variables permits us to obtain the coefficient matrix $\widetilde{P}$, which replaces the requirement of a model, since it contains sufficient information about the dynamics of the to-be-controlled system. Then, the matrix inequality shown in (3.12) is implemented using MATLAB and other external optimization tools are used, in this case we used *Yalmip*. To set up (3.12), it is necessary to define the adequate sizes of $\widetilde{Psi}$ (in this work $N = 2$ and $q = 6$) and $\widetilde{V}$ (with the same dimension as $\widetilde{P}$. It thus remains to define the matrix $\widetilde{C}$ that contains the parameters of the candidate controller. For ease of implementation, one chooses a PI configuration as the candidate controller with the following equations:

$$\begin{aligned}\Delta v_c^d = &-K_1\Delta i_d - K_2\Delta i_q - K_3\Delta v_{dc} - K_4\Delta v_{ac} \\ &- K_5 z_1 - K_6 z_2,\end{aligned} \tag{3.17}$$

$$\begin{aligned}\Delta v_c^q = &-G_1\Delta i_d - G_2\Delta i_q - G_3\Delta v_{dc} - G_4\Delta v_{ac} \\ &- G_5 z_3 - G_6 z_4\ ,\end{aligned} \tag{3.18}$$

where the variables $z_1, ..., z_4$ are obtained by discrete-time integration, that is,

$$\sigma \begin{bmatrix} z_1 \\ z_2 \\ z_3 \\ z_4 \end{bmatrix} = \begin{bmatrix} z_1 \\ z_2 \\ z_3 \\ z_4 \end{bmatrix} + \begin{bmatrix} \Delta v_{dc} \\ \Delta v_{ac} \\ \Delta v_{dc} \\ \Delta v_{ac} \end{bmatrix}\ . \tag{3.19}$$

The controller therefore has the following representation:

$$\underbrace{\begin{bmatrix} -K_1 & -K_2 & -K_3 & -K_4 & -1 & 0 & -K_5 & -K_6 & 0 & 0 \\ -G_1 & -G_2 & -G_3 & -G_4 & 0 & -1 & 0 & 0 & -G_5 & -G_6 \\ 0 & 0 & -1 & 0 & 0 & 0 & \sigma-1 & 0 & 0 & 0 \\ 0 & 0 & 0 & -1 & 0 & 0 & 0 & \sigma-1 & 0 & 0 \\ 0 & 0 & -1 & 0 & 0 & 0 & 0 & 0 & \sigma-1 & 0 \\ 0 & 0 & 0 & -1 & 0 & 0 & 0 & 0 & 0 & \sigma-1 \end{bmatrix}}_{C(\sigma)} \begin{bmatrix} \Delta i_d \\ \Delta i_q \\ \Delta v_{dc} \\ \Delta v_{ac} \\ \Delta v_c^d \\ \Delta v_c^q \\ z_1 \\ z_2 \\ z_3 \\ z_4 \end{bmatrix} = 0.$$

As defined in (3.8), and as exemplified in (3.16), the factorization of $C(\sigma)$ leads to the coefficient matrix $\widetilde{C}$. Finally, the gains $K_1, ..., K_6$ and $G_1, ..., G_6$ are numerically computed by solving (3.12). Although every version of the software is portable enough to work with different versions, in the present work, it might be of interest that we used MATLAB R2021a, YALMIP R20210331, and the standard LMILAB solver available in MATLAB. The latter was used as a default option, but the results were

also corroborated by using SEDUMI 1.1 as a solver. The reader can refer to [24] for more information and more suitable options.

The realization of the controller in terms of a flow diagram is shown in Figure 3.3. In the following sections, we discuss the performance of the proposed data-driven controller with respect to the model-based strategy introduced in the previous section.

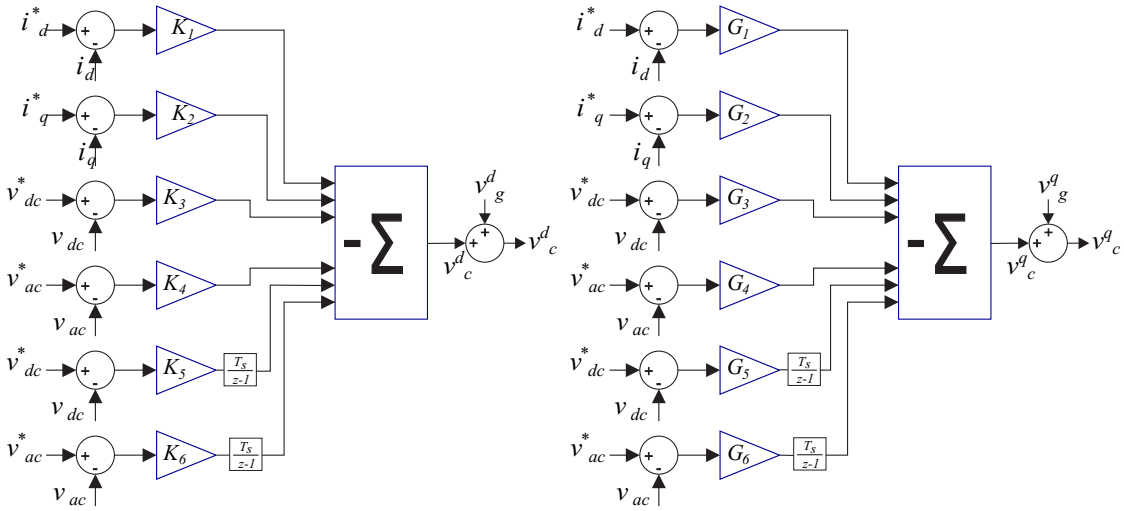

Figure 3.3: Data-driven controller for a VSC-based STATCOM model.

Chapter 4

Results

4.1 Static Synchronous Compensator (STATCOM)

4.1.1 Test System

In order to validate the data-driven controller of a VSC-based STATCOM model, a two areas power system is employed. The test system is simulated in Matlab/Simulink software; it is comprised of a 2-area power system connected by two AC transmission lines and two machines in each area; these test systems are well-known, such as the Kundurs 2-area 4-machine power system. The complete details of the electrical grid can be found in [22]. The single-line diagram can be seen in Figure 4.1. The active power exchange between two areas is around 400 MW, going from area 1 to area 2, and the swing generator corresponds to machine 2, labeled as G2. The STATCOM model is connected to Bus 7 (B7) for controlling the AC bus voltage V_{ac} and the power ratings of the STATCOM can be seen in [33], where a step-up transformer 195kV/230kV is employed to connect it to the grid.

The proposed data-driven control is assessed considering different operating conditions according to the established voltage profile as well as transient faults to analyze power oscillations just after the fault clearing time. All simulations are carried out

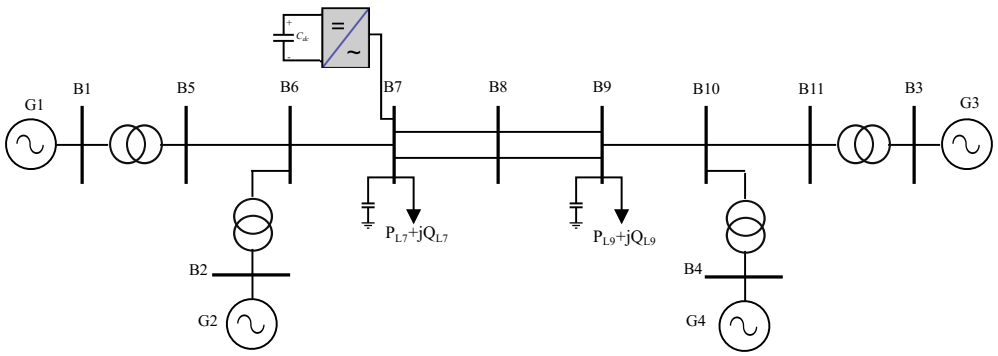

Figure 4.1: Two-area power system [22].

using Matlab/Simulink software, and a time step T_s equal to 1×10^{-4} is used for the implementation of the data-driven controller. The data-driven controller can be set up from the historical data collected from the grid or even from another model-based closed-loop operation of the STATCOM connected to the grid. Therefore, the data-driven controller will guarantee the dynamic performance of the STATCOM according to the rated reactive power because this will be mainly designed to operate to their limits.

The main advantage of the data-driven controller is that it is completely model-free, while its stability and general dynamic performance are equally deterministic, as if it was based on the existence of a completely accurate model of the grid. To account for this fact, we proceed to make a comprehensible comparison between the two scenarios: model-based and model-free. Other advantages include the ability to bypass the issue arising from model uncertainties, which is the typical weakness of any model-based approach. Based on the described advantages, the proposed approach is validated analyzing the performance of a VSC-based STATCOM model, which is compared to the model-based control system under three different scenarios: (a) by using changes in AC reference voltage; (b) by analyzing the voltage recovery after a three-phase fault; (c) power oscillation damping after the fault clearing time. For either, data-driven and conventional models, an average model of the VSC is used. The PPL parameters and grid parameters are kept the same for both types of controllers.

4.1.2 Voltage Step Response

To demonstrate the performance of the proposed method, we first use a test for comparing both model-based and data-driven control, which consists of changing the AC voltage reference V_{ac}. For this scenario, V_{dc}^{*} remains unchanged given that it should be constant according to [32]; this means that I_d and I_q should be effectively compensated for by the controller in order to keep V_{ac} and V_{dc} close to their references.

Figure 4.2a shows the results for different set points of AC voltages. First, the V_{ac} is stepped up from 1.006 to 1.044 p.u. at $t = 2$ s; then, it is also stepped down from 1.044 to 0.98 p.u. at $t = 8$ s; finally, at $t = 12$ s the reference changes from 0.97 to 1.022 p.u. Notice that both controls present similar behavior during the changes of voltage; this can be confirmed with the error of differences shown in Figure 4.2b. Faster response time represents a faster time to reach a new steady-state defined by a particular variable due to reference changes, which can be measured with Δt. Figure 4.3 shows a fair comparison of the model-based controller and the proposed method during the first voltage step shown in Figure 4.2. Notice that Δt_1 corresponds to the time in which the data-driven controller reaches the new steady-state, while Δt_2 is the elapsed time by the conventional model-based control. In conclusion, Δt_1 corresponds to the settling time which is around 0.242 s, whilst Δt_2 is close to 0.426. Based on the results, the VSC-based STATCOM model with a conventional controller takes more time to reach the new steady-state compared to the data-driven controller. Other time steps are also used to analyze the dynamic response of the controller, and these are summarized in Table 4.1.

Figure 4.4 displays the current flowing from the STATCOM to the grid, current components in the dq reference frame. Notice that a change in the voltage reference does not impact the current component i_d significantly as shown in Figure 4.4a, while the second component i_q presents the most noticeable changes due to a voltage change may demand more reactive power, and this will be reflected in the reactive component of the current flowing to the system. Figure 4.5 presents the dynamical performance

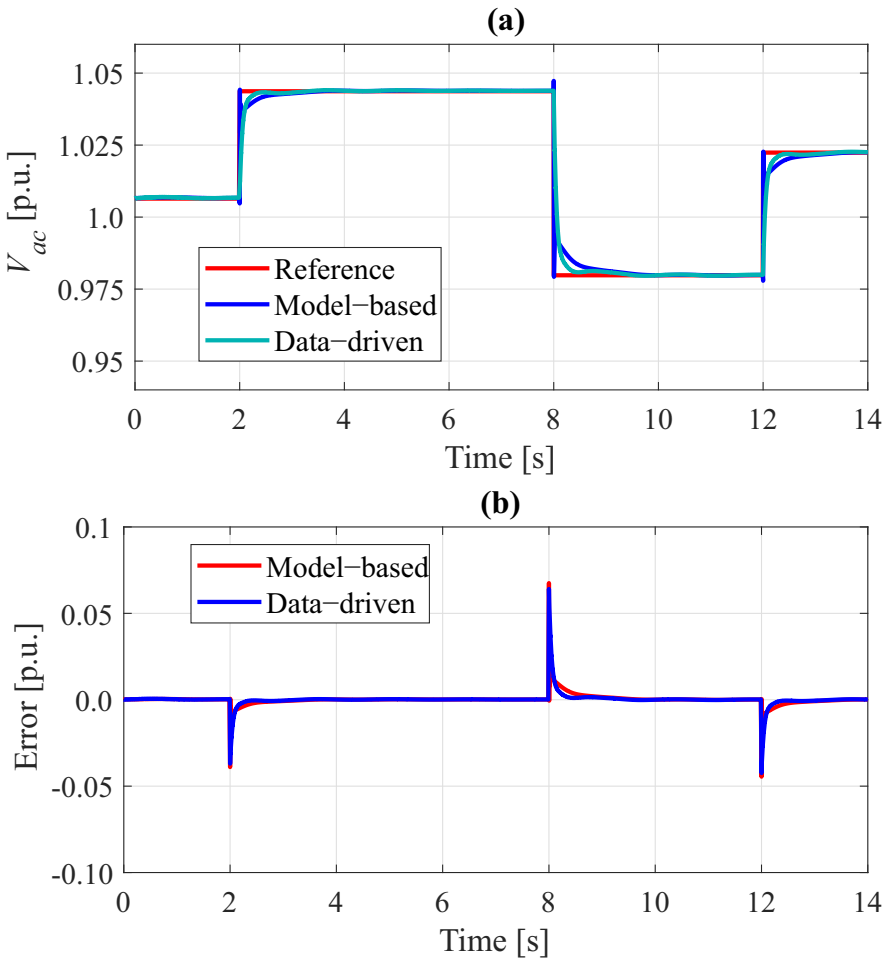

Figure 4.2: Reference changes: (**a**) voltage step comparison and (**b**) errors of differences.

of the reactive power, which is injected into the grid according to the objective of control, that is, a higher voltage will be demanding more reactive power (capacitive) and vice-versa.

4.1.3 Voltage Recovery under Transient Faults

Another subject of interest to assess the dynamic performance of a STATCOM is linked to its ability to provide a fast voltage recovery after a transient event by injecting reactive power, which results in improving the power system stability limits [5, 27]. In this context, the VSC-based STATCOM model using a data-driven controller

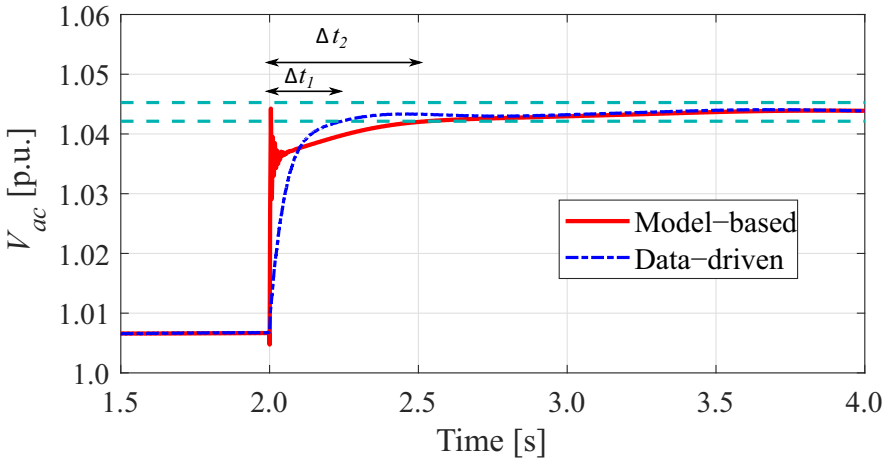

Figure 4.3: Comparison of both control approaches during voltage reference changes.

Table 4.1: Controller performance using different time steps.

Step Time	**Settling Time**	
	Model-Based	**Data-Driven**
$0.25T_s$	0.528	0.243
$0.5T_s$	0.527	0.242
T_s	0.426	0.242
$2T_s$	0.425	0.242

is analyzed because the lack of reactive power may deteriorate the bus voltage values as well the power transfer limits [4]. In this work, the voltage recovery is assessed under two different scenarios: (1) a solid-grounded three-phase fault on Bus 7, and (b) a solid-grounded three-phase fault in one of the parallel transmission lines. For both scenarios, the clearing time corresponds to 100 ms.

Transient Fault on Bus 7

Figure 4.6 shows the dynamic response during a transient fault simulated at Bus 7. Notice that both controllers present small differences in the voltage control. However, a better performance can be observed when the data-driven controller is employed. From Figure 4.6, one can notice that the proposed control presents a higher volt-

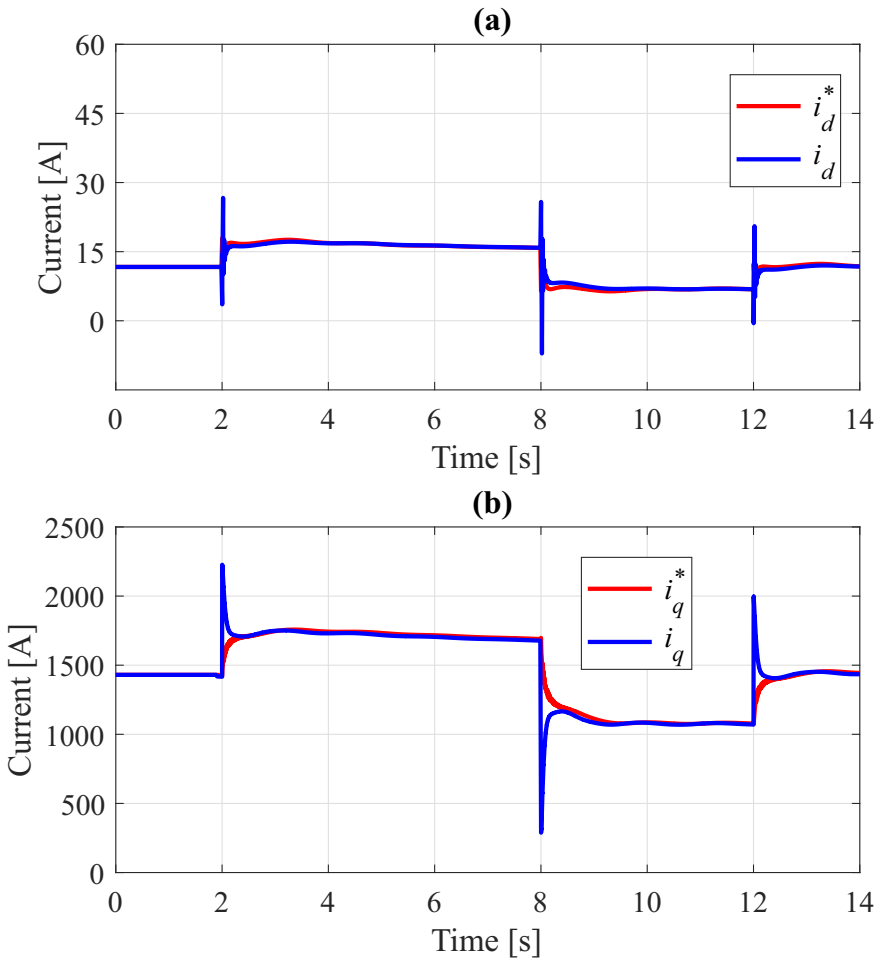

Figure 4.4: Currents of the data-driven controller during changes in the AC reference voltage: (**a**) d-axis current and (**b**) q-axis current.

age overshoot than the model-based control; however, once the fault is cleaned up, the data-driven controller reaches the steady-state faster than the conventional controller. In addition, during any transient fault, the STATCOM will act to maintain the voltage profile according to the AC voltage reference and depending on the fault severity, where sometimes the controller can be saturated. This will be defined by the reactive power requirements during the pre-fault condition, where a larger AC voltage reference will be demanding more reactive power. A fault may also produce a higher overshoot during the transient response, and the controller may be saturated because this has physical limits.

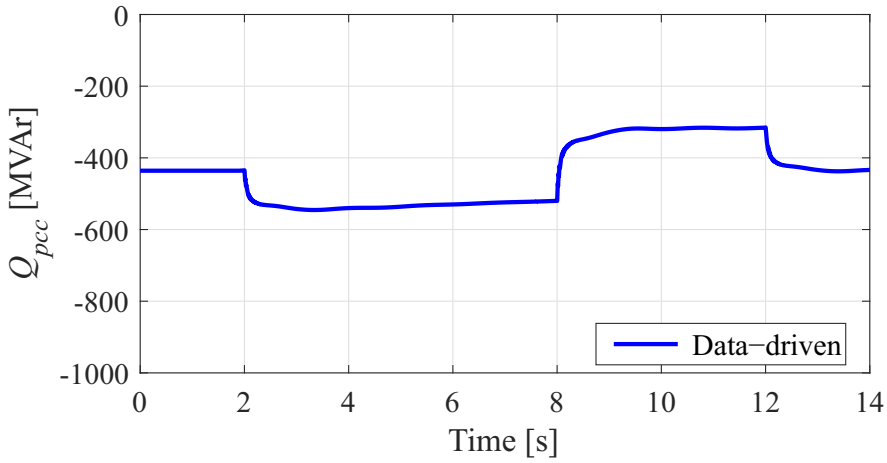

Figure 4.5: Reactive power at PCC using the data-driven controller with changes in the AC reference voltage.

Figure 4.7 confirms the robustness of the proposed approach because the power flows between the interconnected areas, active and reactive powers, present smaller power oscillations than the generated with the conventional control. For instance, Figure 4.7a shows significant differences during the transient behavior of the active power, while Figure 4.7b displays the results of the reactive power.

On the other hand, a STATCOM not only offers the capability to improve the power system efficiency due to its fast dynamic response of voltage control but can also help to mitigate low-frequency power oscillations [16]. For example, Figure 4.8 displays the difference between two rotor angles corresponding to Generator 1 and Generator 2 (defined as slack generator). The results show low-frequency oscillations between both generators when a PSS is used for every generator, except for Generator 4. For all analyzed scenarios, the machine speed deviation is used as an input signal to each PSS. According to the results shown in Figure 4.8, notice that the proposed controller helps to reduce the power oscillations due to the fast dynamic response to recover the AC voltage at the PCC. In addition, the differences shown in Figure 4.8 not only depend on the STATCOM but are also due to other generators. This is the main reason that both responses do not match very well during the transient period. However, notice that after some seconds both controllers have the same behavior; this

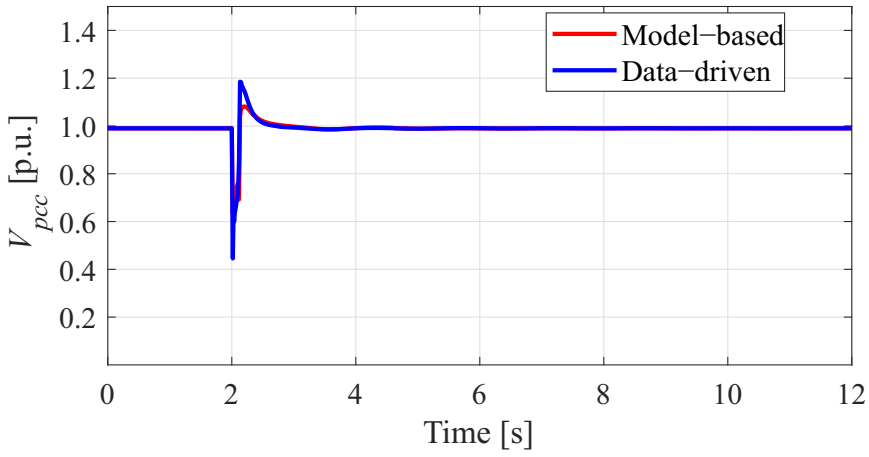

Figure 4.6: Voltage control during transient fault at Bus 7.

means that the power system has reached the new steady-state.

Fault Along the Transmission Line

In this case, a transient fault is analyzed, which is cleaned up by opening the circuit-breakers of the faulted transmission line. The dynamic response corresponding to voltage at the PCC is depicted in Figure 4.9, where significant differences occur between the proposed control scheme and the model-based control. In addition, Figure 4.10 shows the power flow changes after the fault clearing time. The power flow measurements are taken from the non-faulted transmission line. The power transmission losses are increased due to the presence of only one transmission line. The damping capability is highly noticeable in Figure 4.11, which shows the rotor angle difference after the clearing time and due to the change of topology caused by the opening of one transmission line. Figures 4.8 and 4.11 help to confirm the dynamic performance of the data-driven controller in comparison with the conventional model-based controller. Notice that a better performance is exhibited when the STATCOM is controlled by the data-driven approach. Finally, the described results help to confirm the dynamic performance of the data-driven controller in comparison with the model-based controller, where significant differences appear during the transient period. Table 4.2 summarizes the controller performance during transient faults after

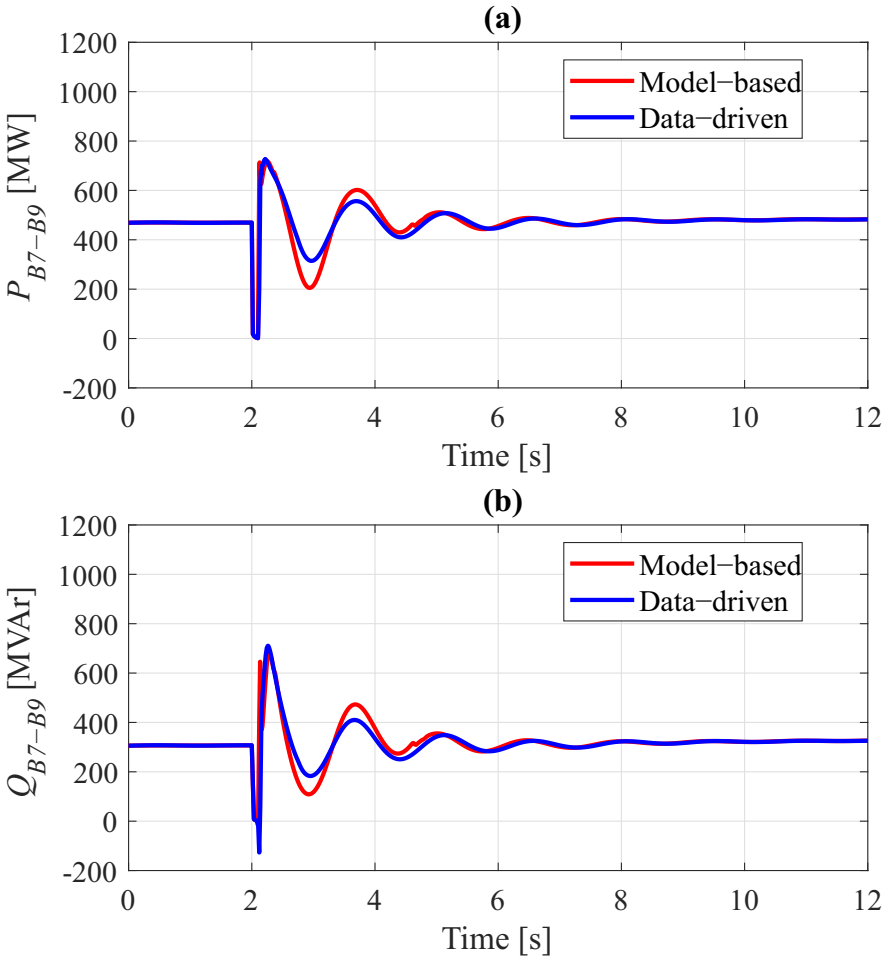

Figure 4.7: Power flow during a fault at Bus 7: (**a**) active power, and (**b**) reactive power.

evaluating different time steps; voltage recovery after the fault clearing time. Finally, considering all analyzed variables, the results showed that the data-driven controller offers better performance during transient events because the resulting power oscillations are smaller in magnitude for all analyzed scenarios.

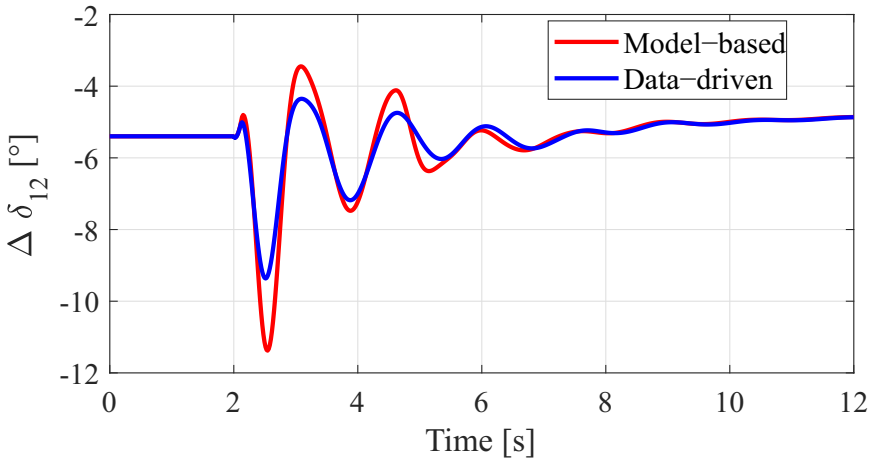

Figure 4.8: Rotor angles during a fault at Bus 7.

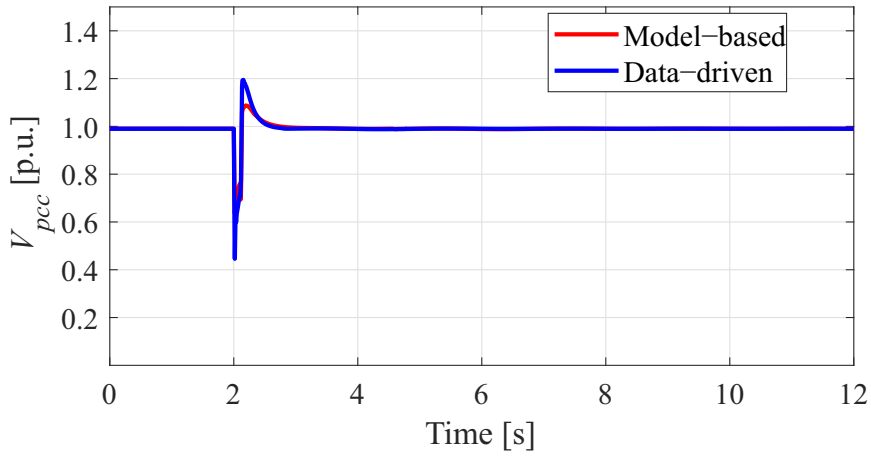

Figure 4.9: AC voltage during a fault on the transmission line.

4.1.4 Load Shedding Assessment

One of the last resources to mitigate electric power generation deficiency is load shedding. It consists of disconnecting the less essential loads connected to the grid. An inequality between power generation and consumption affects the power system frequency leading to a collapse [1]. Load shedding is a common practice that can be either beneficial or detrimental to the power system stability. The disconnection of considerable sizing loads creates a mismatch between mechanical and electrical power, causing a positive power acceleration that can lead to power system instability.

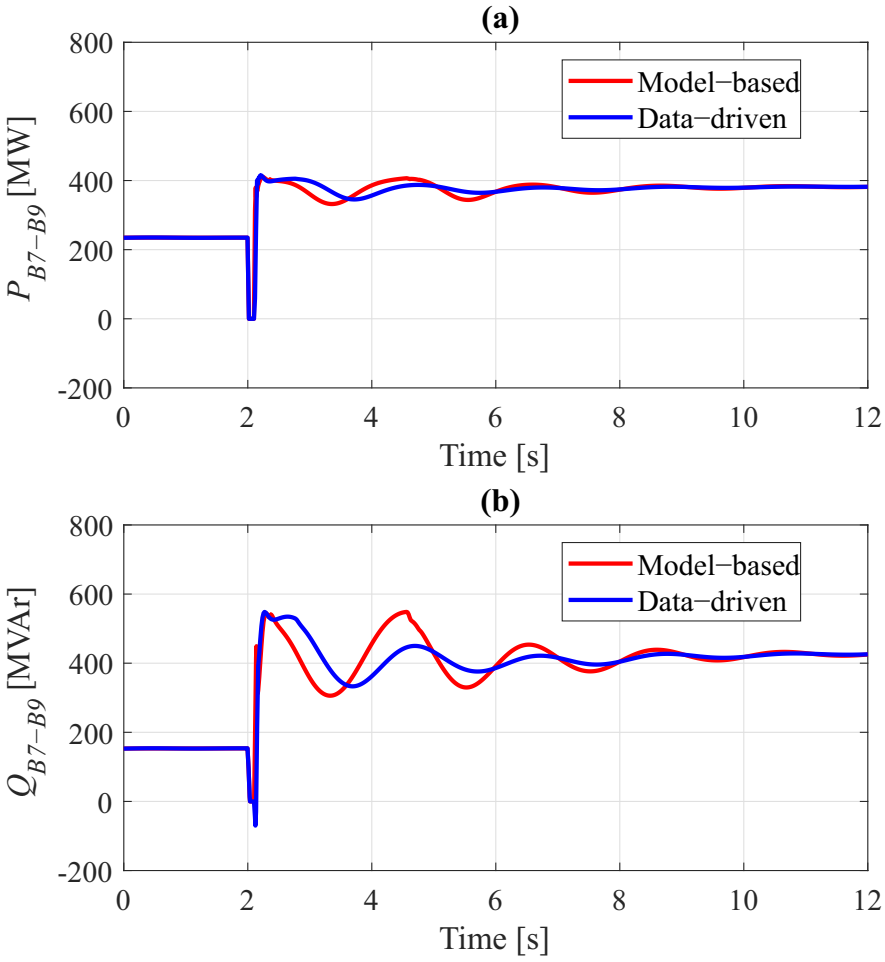

Figure 4.10: Power flows during transient fault and topology change: (**a**) active power, and (**b**) reactive power.

To assess the performance of the STATCOM after a load shedding, a 200 MW load is disconnected from Bus 9. The load shedding decreases the power flow between the two areas bringing a new condition to the generation (rotor angles). Figures 4.12 and 4.13 show the comparison between the transient response of the model-based and data-driven controllers. Regarding the real and reactive power flows shown in Figure 4.12, both controllers present quite a similar performance. The transient response of the AC voltage shown in Figure 4.13 reaches a peak voltage of 1.03 p.u. when the data-driven controller is employed. That voltage is a bit higher than that produced by the model-based controller but both controllers match very well due to both producing the same magnitude on the first oscillation and almost the same settling time. The

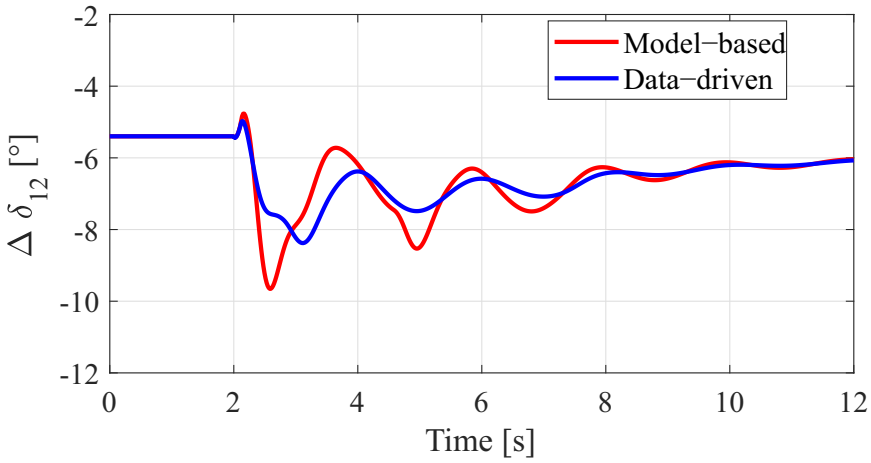

Figure 4.11: Rotor angles during transient fault and topology change.

Table 4.2: Controller performance during transient faults using different time steps.

Step Time	**Overshoot**		**Settling Time**	
	Model-Based	**Data-Driven**	**Model-Based**	**Data-Driven**
$0.1T_s$	0.100	0.21	1.050	0.84
$0.5T_s$	0.093	0.21	1.030	0.78
T_s	0.090	0.21	0.894	0.83
$2T_s$	0.090	0.20	0.894	0.83

reactive power injected by the STATCOM can be shown in Figure 4.13, where both controllers present a similar behavior. Notice that the load shedding will demand less reactive power as expected.

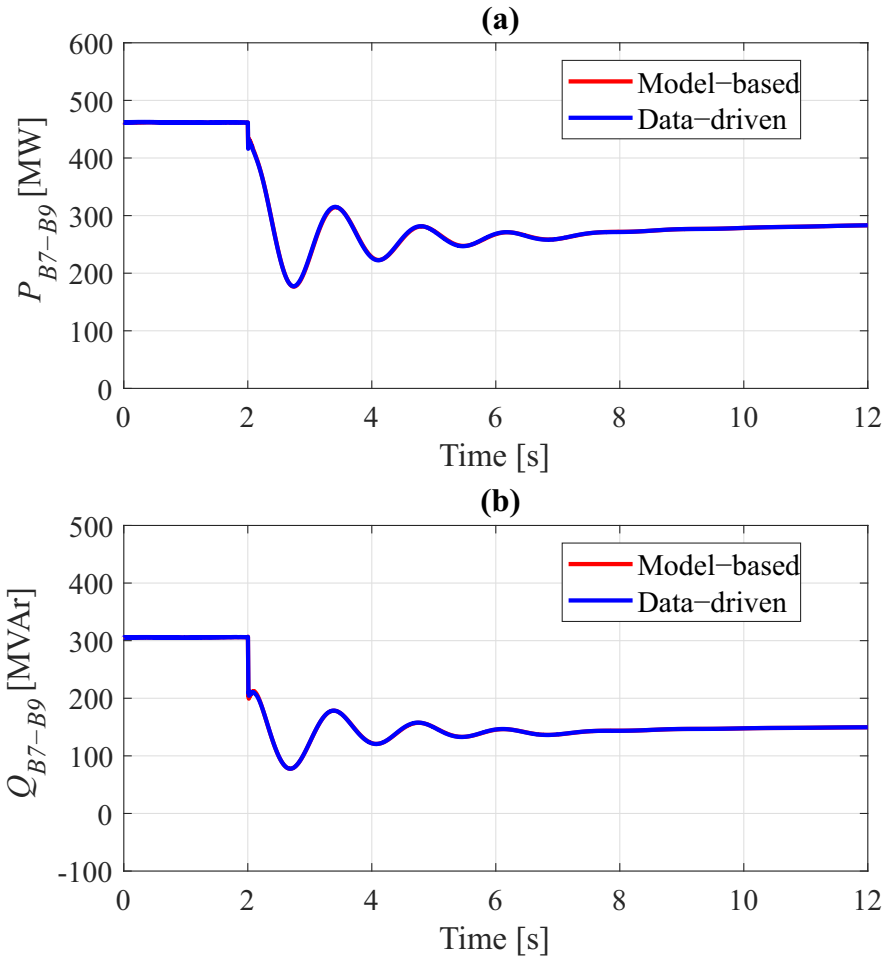

Figure 4.12: Power flows during load shedding: (**a**) active power, and (**b**) reactive power.

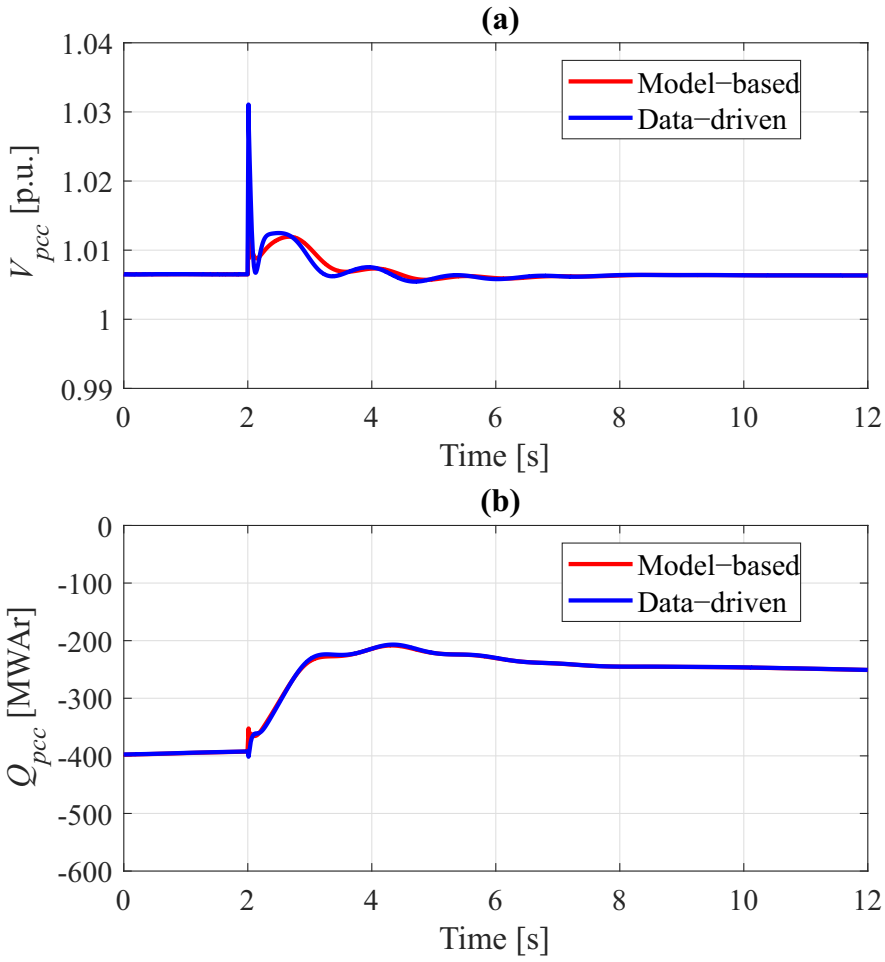

Figure 4.13: STATCOM: (**a**) AC voltage, and (**b**) reactive power during load shedding.

4.2 Battery Energy Storage System (BESS)

To analyze the performance of the data-driven controller compared to the model-based, the same two areas power system is used as in the STATCOM study case. The BESS remains connected to bus B7 as shown in Fig. 4.1. The BESS is a battery model represented by a DC source, which means it can deliver and absorb real power. The active power exchange remains around 400 MW but in this case, the total power is the sum of Generator 1, Generator 2 (swing), and BESS during its discharge period. Notice that the BESS can deliver limited power, for this study case, it is assumed that the times of power delivered by the BESS are short enough. The BESS model-free is compared to the model-based under three different scenarios: (a) by changes is real power reference, (b) by analyzing the power delivery after a three-phase fault; (c) power damping after the fault clearing time. The sampling rate T_s for the model-based control is kept the same as in the STATCOM. The PLL parameter remains unchanged.

4.2.1 Active Power Step Response

To assess the performance of the model-based controller, the first test compares it to the model-based by changing the active power reference P_{ac}. For this case, V_{ac}^{*} remains unchanged and I_d should be compensated. Figure 4.14a shows the result of all changes due to the settings of the active power. First, the P_{ac} is set to 50 MW, so at 5 s, it is stepped up to 100 MW; then at 10 s stepped down to 75 MW; finally at 15 s stepped down to 50 MW. The active power changes present similar behavior for both model-based and model-free controllers. Fig. 4.14b shows the error differences of both controllers' responses against the reference setpoints, showing that the dynamic response of both systems is quite similar.

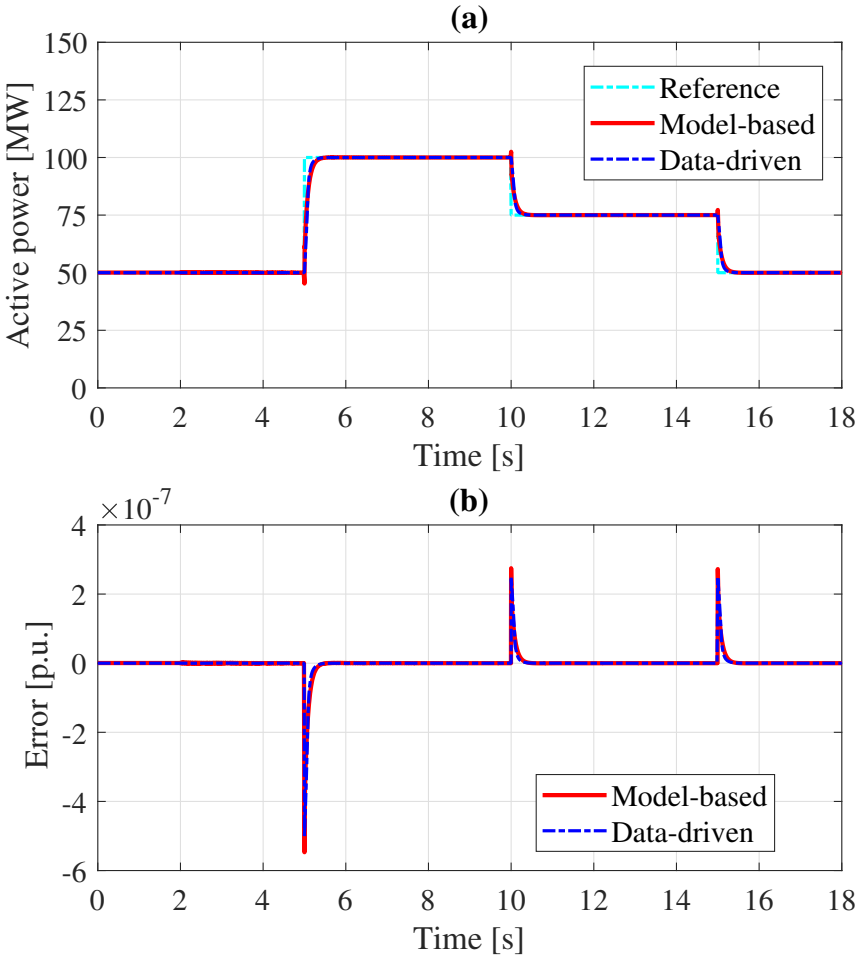

Figure 4.14: Reference changes: (**a**) active power step comparison and (**b**) errors of differences.

Taking a closer look at the active power step response the improvements seem to be better in Fig. 4.15. The data-driven controller reaches the new setpoint approximately at 0.2 s just before the model-based controller. The current components, in the *dq* reference frame, flowing from the BESS are shown in Fig.4.16. Since I_d and I_q depend on the outer loop inputs, both variables experience transient conditions due to all dynamics imposed by the model. However, the tracking of current is guarantee by the proposed controller even when large changes occur caused by non-fault transient conditions.

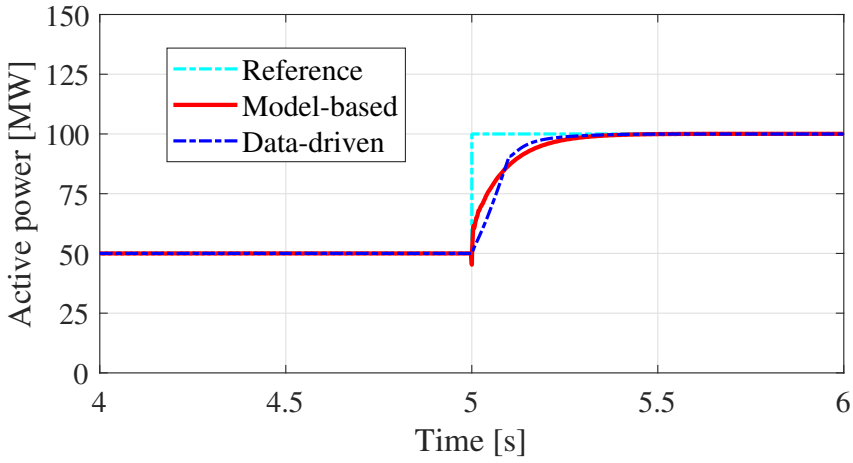

Figure 4.15: Comparison of both controllers during active power reference changes.

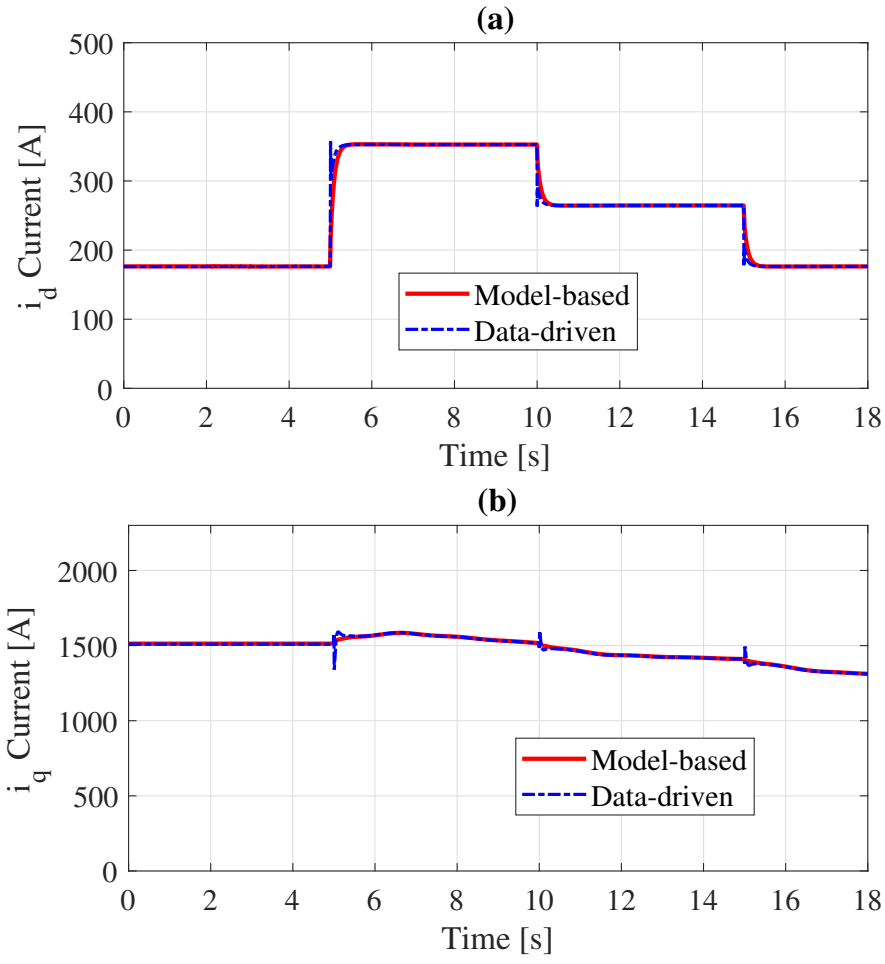

Figure 4.16: I_d and I_q changes due to active power step changes.

4.2.2 Load Shedding Assessment

The load shedding performance related to a BESS is very important because two aspects can be assessed: the voltage recovery and the active power reference changes to improve the dynamic response of the overall power system. By controlling the active power delivered by a BESS according to the grid energy demand, it can be very promising in case that there is an unbalance condition of demand/supply. To validate the model-free VSC-based BESS model, two comparison are carried out: a) voltage recovery and b) active power reference change when load is shed, that is, the active power changes caused by the load shedding is absorbed by the BESS.

To cope with the load shedding assessment, 20% of the load connected to Bus 9 is disconnected, resulting in a power transfer decrease between the two areas. The load decrements create unbalance conditions in the grid, the swing generator and the BESS will have new set-points in order to have a balance between power generation and demand. In this context, the unbalance produced during the load shedding is addressed by the BESS, that is, the power delivery to the grid should be reduced in the same proportion as the load shedding. Results of the load shedding can be seen in Fig. 4.17a), where the load tripping was simulated at 10 s. In order to highlight the main differences between both analyzed controllers, the transient period is studied for the load shedding scenario; the dynamic response of the load tripping is evaluated before and after the change. Figure 4.17b) shows the dynamic response between 8 s and 12 s. This figure helps to confirm that the data-driven approach versus the model-based controller can reach faster the reference, which means a settling time smaller.

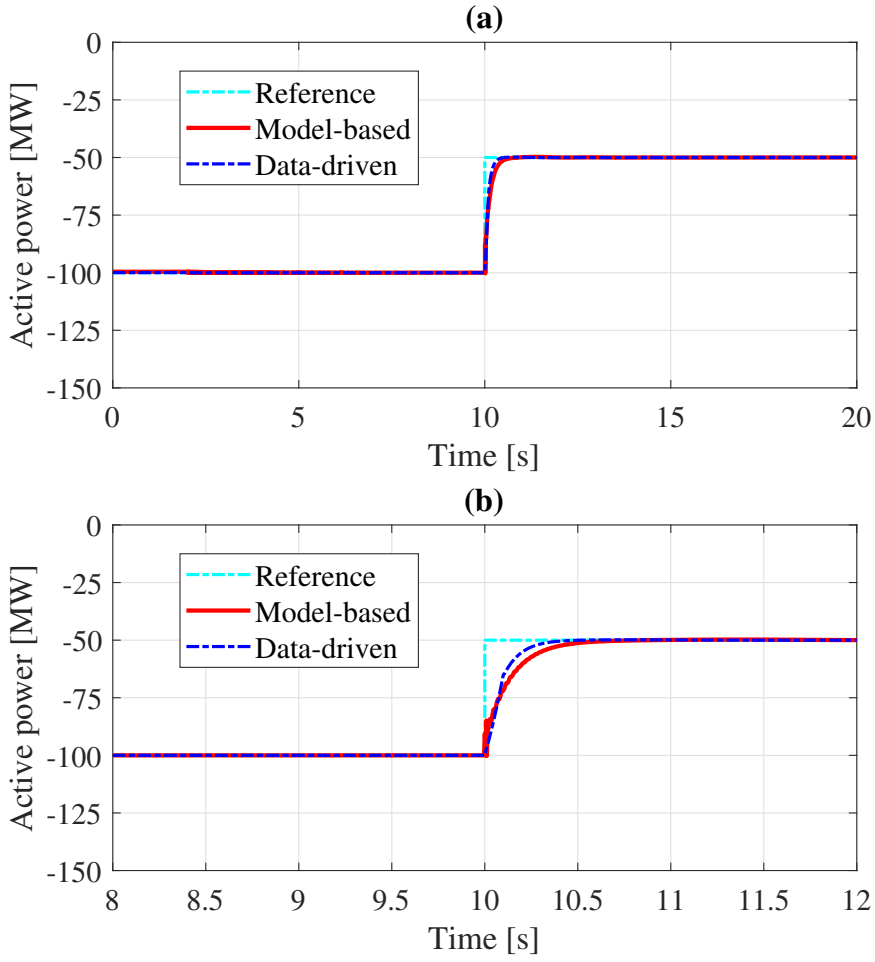

Figure 4.17: Active power delivery by the BESS with a reference change at 10s

The load disconnection not only changes the active power set-point at the BESS but also creates a transient condition that will be reflected into the AC voltage. In this sense, the dynamic performance of the AC voltage is analyzed by comparing the model-based and data-driven controllers. Remembering that the load tripping occurred at 10 s, it hopes a transient response into the AC Voltage will be damped over time. Figure 4.18 corresponds to the AC voltage during the load shedding; notice that both controllers have an overshoot during the transient period that is within the admissible range but the data-driven approach generates a higher overshoot than the produced by the model-based controller. Additionally, both controllers present quite similar results just after 2 s of the load shedding. Based on the results, it can be concluded that the data-driven controller is faster than the model-based controller to

reach the new steady state. This scenario helps to confirm the excellent performance of the proposed controlled under transient events. Additionally, both con

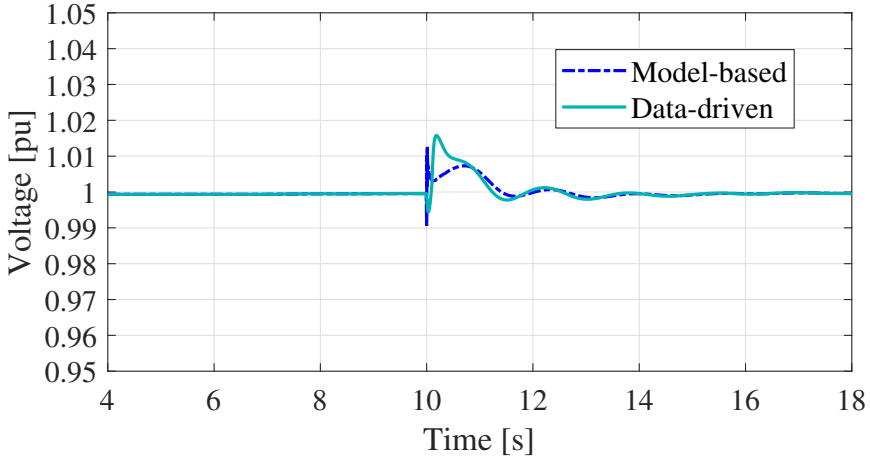

Figure 4.18: AC voltage performance comparison between model-based and data-driven controller

Other important variables are I_d and I_q since the entire control is determined by them. Load shedding causes a transient condition both in active power and AC voltage; therefore, I_d and I_q should experience some changes during some time. Fig. 4.19 shows the dynamic response of currents in the dq reference frame. Fig. 4.19(a) presents the results of I_d both data-driven and model-based controllers, where it can notice that the settling time of the data-driven approach is around 0.25 s while the model-based controller is approximately 0.5 s. Results confirm that I_d produced by the data-driven approach shows a faster response compared to the model-based controller. On the other hand, Fig. 4.19(b) shows the dynamic response for I_q where both controllers perform similar.

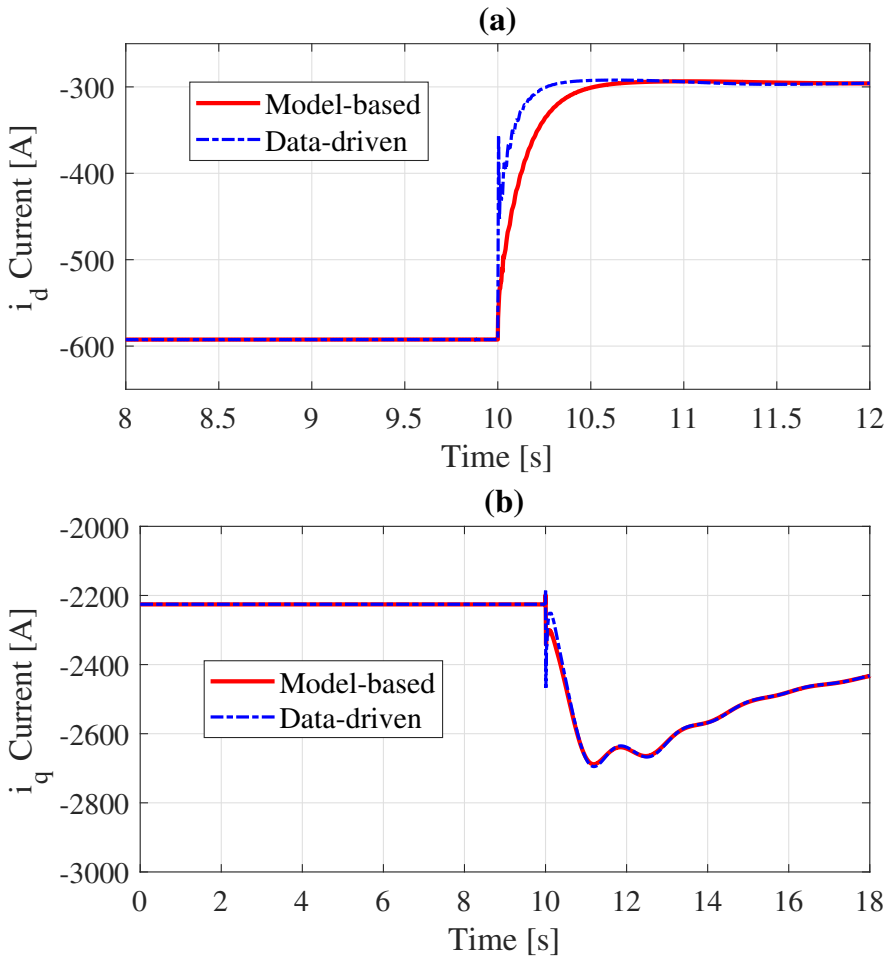

Figure 4.19: Active power delivery by the BESS with a reference change at 10s

4.3 VSC-HVDC Link

4.3.1 Test System

The use of voltage source converters has also been employed in high-voltage direct current (HVDC) transmission, which is referred to as VSC-HVDC transmission. This system shows particular advantages (emulates an inertial effect helping to limit the change rate of frequency), especially for connecting wind power plants to the electrical grids. In this context, the proposed control approach is applied to VSC-HVDC transmission. To assess the proposed data-driven approach, the same two-area power system is used but now considering an HVDC link as shown in Fig. 4.20. VSC-HVDC comprises two converters on each side of the DC line, one of them controls active power on the DC link, while the second one is used for DC voltage control. To perform the analysis, three types of tests are undertaken which include reference voltage changes, faults, and load shedding.

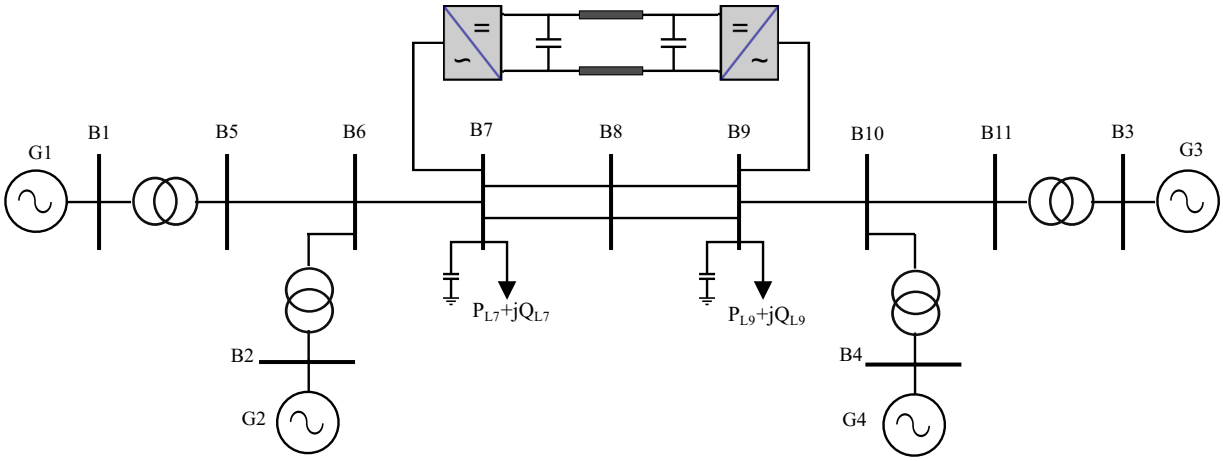

Figure 4.20: Two-are power system using VSC-HVDC power transmission

4.3.2 Active Power Step Response

One of the main goals of a VSC station is to control the transmitted active power into the DC link. This allows controlling the power flow according to the neediness of

the interconnected areas. Active power is controlled by the rectifier converter, which must be able to meet different operating points according to the setpoints demanded by the interconnected grids. In this context, the proposed controller is evaluated considering multiple references changes of active power. To cope with this analysis, the converter connected to Bus 7 is set to be the rectifier controlling the active power through the HVDC link, and it is also used for controlling the AC voltage. The VSC connected to Bus 9 represents the inverter, which is employed to control both DC and AC voltage. For example, three different operating points were studied to analyze the dynamic performance of the proposed controller. Figure 4.21 shows the results for an active power step-change simulated at 5 seconds, from 50 MW to 100 MW. After that, at 10 seconds the active power goes down from 100 MW to 75 MW. Finally, the active power steps down from 75 MW to 50 MW at 15 seconds. Notice that both analyzed controllers present s quite similar behavior and follow accurately the active power setpoints.

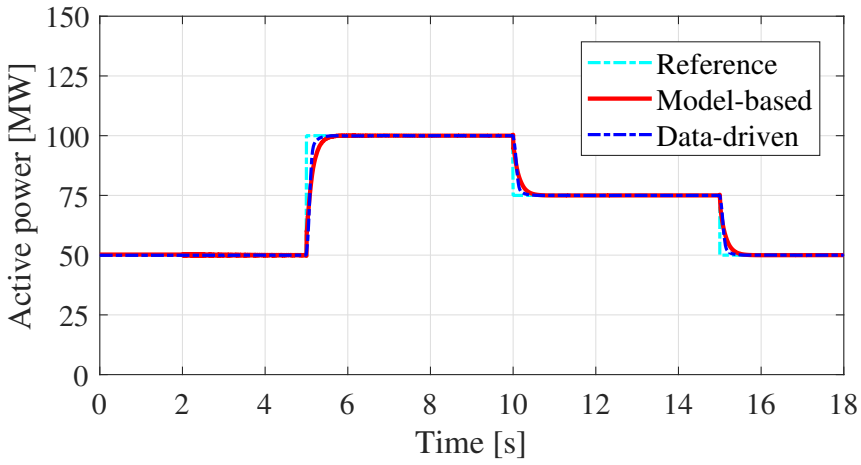

Figure 4.21: Active power demanded by the VSC-rectifier with reference changes at 5s, 10s and 15s.

From Fig. 4.22, it can clearly observe the main difference of both implemented controllers during reference changes of active power. Notice that the data-driven controller shows better performance during active power changes compared to the model-based. In addition, the data-driven controller reaches the new steady-state at

0.25 s showing a faster than the model-based controller.

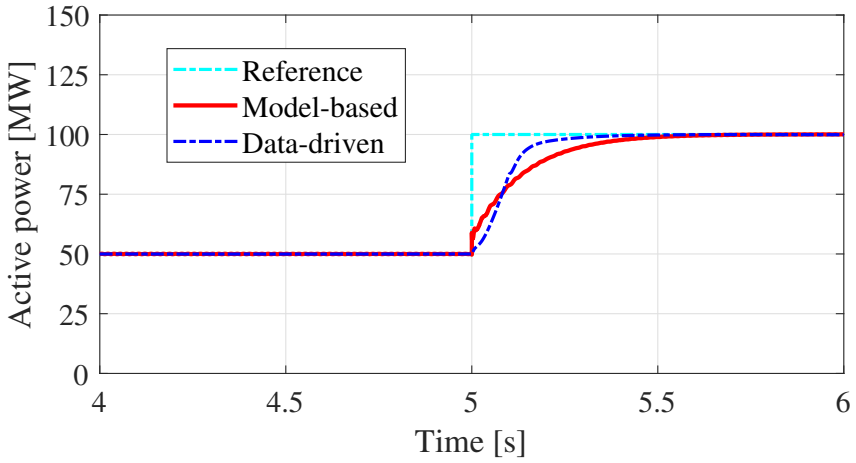

Figure 4.22: Active power step at 5s.

By using the same sequence of changes shown in Fig. 4.21, the dynamic response of the AC voltage is examined. The AC voltage is controlled by the rectifier side and its dynamic response can be seen in Fig. 4.23, where the data-driven controller shows small peaks during the reference changes of active power. On the other hand, the model-based controller presents a dissimilar behavior because the transient response of the AC voltage is almost unnoticeable when the active power changes. These results help to confirm the effectiveness of the proposed controller.

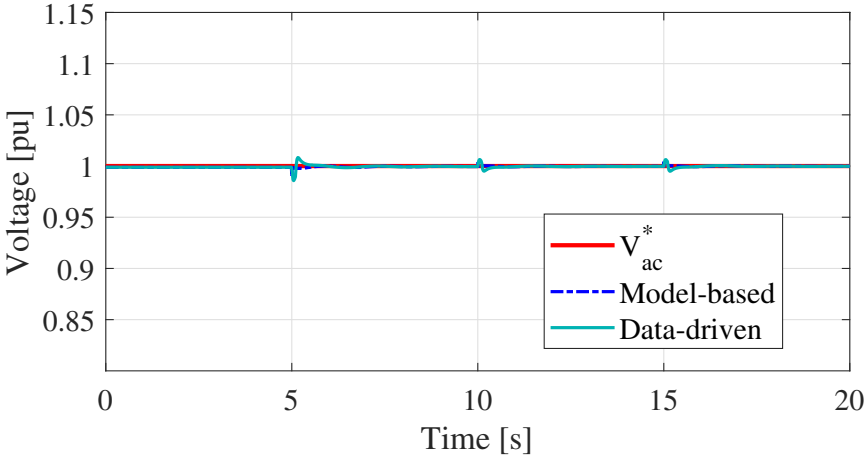

Figure 4.23: AC voltage comparison on the rectifier side.

The dynamic behavior of the rectifier is analyzed using the dq reference frame where the current components are shown on Fig. 4.24. Figure 4.24(a) shows the step response of d-axis current I_d which is related to the active power response. The same figure presents the comparison results of both controllers employed. It can notice that d-axis current based on data-driven not only shows a similar but also yields a faster response compared to the model-based controller, which is around 0.2 seconds. In the same way, the q-axis currents of both controllers were compared during the active power step changes.

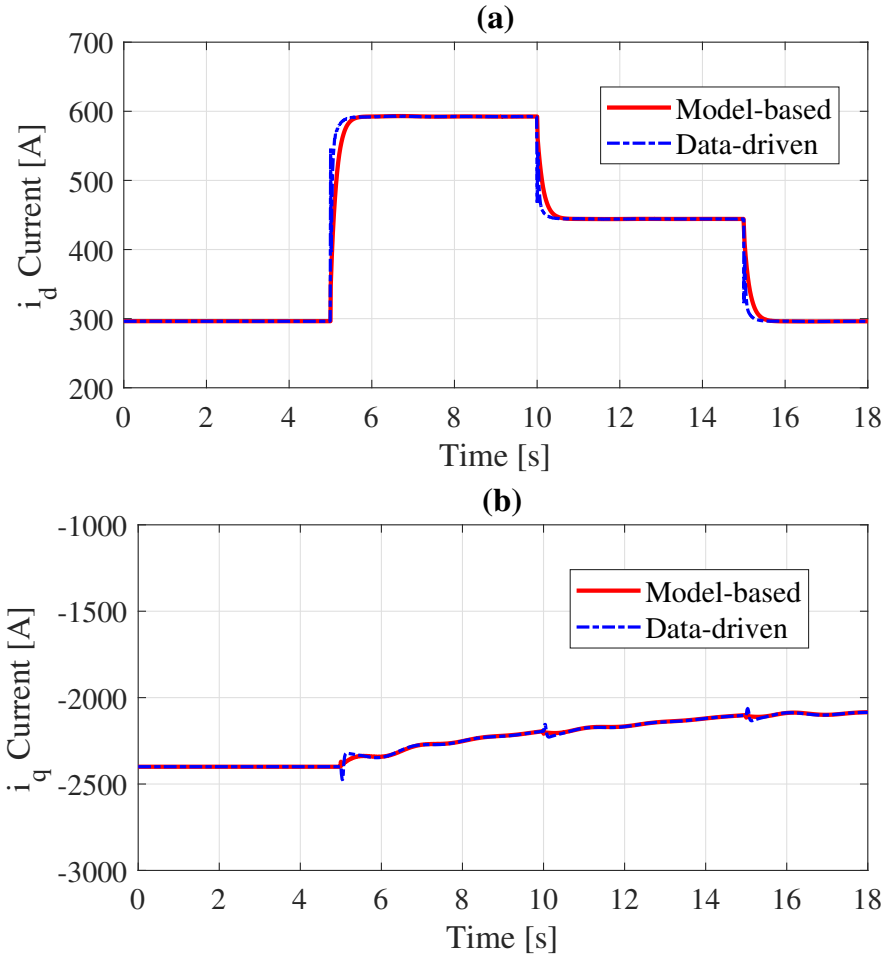

Figure 4.24: I_d and I_q changes due to active power step changes.

On the other hand, the control objective of the VSC station operating as an inverter is to maintain the DC voltage into the DC link. Figure 4.25 displays the dynamic performance of both studied controllers. Note that both controllers show

a dynamic performance caused by the active power changes, where the settling time between the data-driven and the model-based controllers is quite similar, but the dynamic response is different because small oscillations appeared when the data-driven is applied. In addition, the model-based controller shows a less oscillatory response due to the internal PID tuning, but both controllers exhibit a similar overshoot.

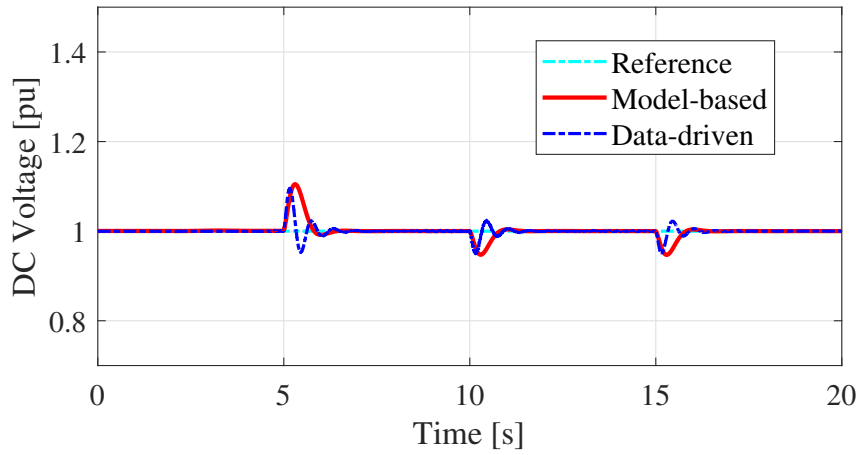

Figure 4.25: DC voltage comparison on the inverter side.

The AC voltage response of the inverter-side is shown in Fig. 4.25. In this case, both controllers yielded a quite similar dynamic response, where small changes occur during the simulated active power changes.

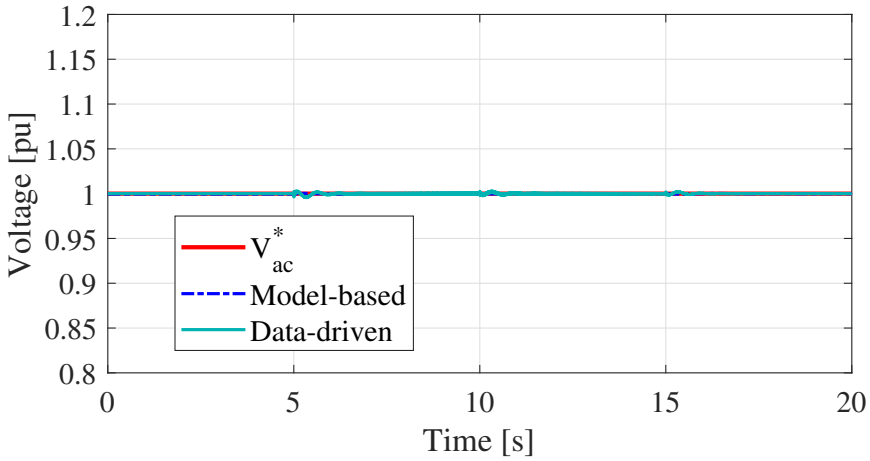

Figure 4.26: AC voltage comparison on the inverter side.

This chapter presented a detailed comparison between the model-based controller and the data-driven controller. The tests were performed by utilizing the data-driven controller in multiple devices such as STATCOM, BESS, and an HVDC transmission line. Each test was evaluated with different types of perturbations depending on the type of device used, which produced different dynamic responses to the involving variables such as AC voltage, DC voltage, active power, etc.

Given the fact, the data-driven controller is based on the model-based controller dynamic response and even though data-driven controller has proven to be faster, it wont replace the main controller but can be used as an auxiliary option to improve the dynamic response. The data-driven controller has some advantages over the model-based within which are a faster response, more defined stability criteria. Some disadvantages are the dependence on other systems and sometimes the implementation can be more complex.

Analyzing the STATCOM, the results showed that the data-driven is a solid option to complement the model-based controller. The test carried out showed that the proposed controller is very capable of showing to be a robust and fast controller compared to the conventional. The two controlled variables were the AC voltage and DC voltage. The AC voltage control was possible by means of reactive power injection and the proposed control showed a considerably faster response compared to the model-based controller.

The BESS performed similarly to the STATCOM. The active power control was fast with a short transient time. The AC voltage was kept constant and showed a solid recovery when the system was in transient condition. The VSC-HVDC link is more complex than the other devices (BESS and STATCOM) since it has two converters. The rectifier using the data-driven controller exhibited a prominent response in comparison with the model-based, unlike the inverter that showed a slightly worse behavior. The reason lies in the tuning of the data-driven controller. Since there is a connection between two converters that were tuned separately, a retuning must occur to get an optimal dynamic response.

In conclusion, the data-driven controller performance compared to the model-based controller under several assessments presented a fast dynamic response under transient conditions proving to be a solid control approach for use in VSC. Results showed a fast voltage control, active power, and even improved response for power oscillation damping. FACTs in general, play an essential role in modern power grids. The use of renewable energy sources and the need for long-distance bulk transmission can partially be front faced with new technologies such as FACTs and HVDC power transmission.

Chapter 5

Conclusions

The operation and control of a VSC model were studied by introducing a novel control approach based on data-driven. The theoretical fundamentals were addressed to implement the control strategy in AC-DC power grids. The proposed data-driven control was initially assessed by analyzing a VSC-based STATCOM. The data-driven controller was evaluated in BESS to comply with particular requirements of power injection to the grid. An HVDC transmission system was modeled by employing data-driven at both VSC stations to control the active power flow into the DC link. For each study case, all advantages and drawbacks were highlighted considering several operating points. The validity of the control strategy was compared against to model-based controller for the reported scenarios showing good performance.

The data-driven controller was designed following certain parameters such as robustness, speed, stability criterion, and capturing the grid dynamic characteristics within itself. A new controller with better performance is the main contribution of this work. The data-driven controller was assessed under multiple tests using three VSC-based devices. These tests included step response, voltage control under transient conditions and load shedding in which the data-driven control was compared to the model-based control. The new control design was proven to be effective throughout the multiple tests to which it was subjected, being faster and having a better

performance than the model-based control in most of them. Apart from multiple tests and comparisons, the main contribution of this thesis is the development of model-free control which contains the dynamics of the electrical grid within itself.

Future work

- The previously work focused mainly on the use of VSC applied to HVDC and FACTS, but VSC are also the basis for the integration of renewable energy systems. A study of data-driven control applied to devices such as photovoltaic systems, and wind power would be of the utmost importance in order to improve the performance of said devices.

- The use of auxiliary control loops isn't addresses on the this work, but this type of controls loops are well-known for improving system performance, the data-driven control could be fed back with an auxiliary control loop to improve it dynamic response.

- VSC are capable of working connected to weak grids, it would be interesting to study an VSC-HVDC link in which the Short-Circuit Ratio (SCR) of the interconnected areas differ by a high amount to see the performance of the data-driven control.

Bibliography

[1] Adel A. Abou, A. Zein El-Din, and Sh R. Spea. "Optimal load shedding in power systems". In: *2006 Eleventh International Middle East Power Systems Conference*. Vol. 2. 2006, pp. 568–575.

[2] L. de Andrade and T. Ponce de Leão. "A brief history of direct current in electrical power systems". In: *2012 Third IEEE HISTory of ELectro-technology CONference (HISTELCON)*. 2012, pp. 1–6. DOI: 10.1109/HISTELCON.2012.6487566.

[3] Michael P. Bahrman and Brian K. Johnson. "The ABCs of HVDC transmission technologies". In: *IEEE Power and Energy Magazine* 5.2 (2007), pp. 32–44. ISSN: 15407977. DOI: 10.1109/MPAE.2007.329194.

[4] Pollen Barua and Muhammad Quamruzzaman. "Steady State Voltage Vulnerability and Stability Limit Analysis of Bangladesh Power System Using STATCOM as a Shunt Compensator". In: *2018 4th International Conference on Electrical Engineering and Information Communication Technology (iCEEiCT)*. 2018, pp. 1–4. DOI: 10.1109/CEEICT.2018.8628122.

[5] Sarita Bhole and Prateek Nigam. "Improvement of Voltage Stability in Power System by Using SVC and STATCOM". In: *International Journal of Advanced Research in Electrical, Electronics and Instrumentation Engineering* 04 (Feb. 2015), pp. 749–755. DOI: 10.15662/ijareeie.2015.0402035.

[6] Matthias K Bucher et al. "Multiterminal HVDC Networks — What is the Preferred Topology ?" In: 29.1 (2014), pp. 406–413.

[7] CFE. *Informe Anual*. Tech. rep. Mexico, 2015.

[8] Napat Chatrung. "Battery Energy Storage System (BESS) and Development of Grid Scale BESS in EGAT". In: *2019 IEEE PES GTD Grand International Conference and Exposition Asia (GTD Asia)*. 2019, pp. 589–593. DOI: 10.1109/GTDAsia.2019.8715953.

[9] P Cominos and N Munro. "PID controllers: recent tuning methods and design to specification". In: *IEE Proceedings-Control Theory and Applications* 149.1 (2002), pp. 46–53.

[10] Daniel Pérez Dorantes, José Luis Monroy Morales, and Máximo Hernández Ángeles. "A filter design methodology of a VSC-HVDC system". In: *2013 IEEE International Autumn Meeting on Power Electronics and Computing (ROPEC)*. 2013, pp. 1–6. DOI: 10.1109/ROPEC.2013.6702737.

[11] Mircea Eremia, Chen-Ching Liu, and Abdel-Aty Edris. "Static Synchronous Compensator – Statcom". In: *Advanced Solutions in Power Systems: HVDC, FACTS, and Artificial Intelligence*. 2016, pp. 459–525. DOI: 10.1002/9781119175391.ch8.

[12] Mircea Eremia, Chen-Ching Liu, and Abdel-Aty Edris. "Static Synchronous Compensator – Statcom". In: *Advanced Solutions in Power Systems: HVDC, FACTS, and Artificial Intelligence*. 2016, pp. 459–525. DOI: 10.1002/9781119175391.ch8.

[13] Nikolas Flourentzou, Vassilios G. Agelidis, and Georgios D. Demetriades. "VSC-Based HVDC Power Transmission Systems: An Overview". In: *IEEE Transactions on Power Electronics* 24.3 (2009), pp. 592–602. DOI: 10.1109/TPEL.2008.2008441.

[14] Raymond F Gardner. *Introduction to Plant Automation and Controls*. CRC Press, 2020.

[15] Guan-Chyun Hsieh and J.C. Hung. "Phase-locked loop techniques. A survey". In: *IEEE Transactions on Industrial Electronics* 43.6 (1996), pp. 609–615. DOI: 10.1109/41.544547.

[16] Weihong Huang and Kai Sun. "Optimization of SVC settings to improve post-fault voltage recovery and angular stability". In: *Journal of Modern Power Systems and Clean Energy* 7.3 (2019), pp. 491–499. DOI: 10.1007/s40565-018-0479-0.

[17] M. Imhof and G. Andersson. "Dynamic modeling of a VSC-HVDC converter". In: *2013 48th International Universities' Power Engineering Conference (UPEC)*. 2013, pp. 1–6. DOI: 10.1109/UPEC.2013.6714935.

[18] Markus Imhof. "Voltage Source Converter Based HVDC - Modelling and Coordinated Control to Enhance Power System Stability". PhD thesis. ETH Zurich, 2015. ISBN: 9783906327112. URL: https://doi.org/10.3929/ethz-a-010525485.

[19] N. M. Kirby. "HVDC system solutions". In: *Proceedings of the IEEE Power Engineering Society Transmission and Distribution Conference* (2012), pp. 1–3. ISSN: 21608555. DOI: 10.1109/TDC.2012.6281583.

[20] E. Kontos et al. "Impact of HVDC Transmission System Topology on Multiterminal DC Network Faults". In: *IEEE Transactions on Power Delivery* 30.2 (2014), pp. 844–852. ISSN: 08858977. DOI: 10.1109/TPWRD.2014.2357056.

[21] S. Kumaravel et al. "Genetic algorithm based PI tuning of VSC-HVDC system and implementation using OPAL-RT". In: *TENCON 2017 - 2017 IEEE Region 10 Conference*. 2017, pp. 2193–2197. DOI: 10.1109/TENCON.2017.8228225.

[22] Prabha Kundur. *Power System Stability and Control*. Vol. 23. 1994, p. 739. ISBN: 9780070635159. DOI: 10.1049/ep.1977.0418.

[23] Chi Li et al. "Stability Analysis of Power Systems With Multiple STATCOMs in Close Proximity". In: *IEEE Transactions on Power Electronics* 35.3 (2020), pp. 2268–2283. DOI: 10.1109/TPEL.2019.2931891.

[24] J. Löfberg. "YALMIP : A Toolbox for Modeling and Optimization in MATLAB". In: *In Proceedings of the CACSD Conference*. Taipei, Taiwan, 2004.

[25] Massimo Mazzanti, Giovanni. Marzinotto. "Extruded Cables for High Voltage Direct Current Transmission". In: (2013).

[26] M. Mobarez et al. "A novel control approach for protection of multi-terminal VSC based HVDC transmission system against DC faults". In: *2015 IEEE Energy Conversion Congress and Exposition, ECCE 2015* 52.5 (2015), pp. 4208–4213. DOI: 10.1109/ECCE.2015.7310254.

[27] Michael Neutz. "Power Quality". In: *Voltage Stabilisation for Industrial Grids and Wind Farms with STATCOM*. ABB, 2013, p. 38.

[28] Hyeokjin Noh et al. "STATCOM with SSR damping controller using geometric extraction on phase space reconstruction method". In: *International Journal of Electrical Power & Energy Systems* 120 (2020), p. 106017. ISSN: 0142-0615. DOI: https://doi.org/10.1016/j.ijepes.2020.106017. URL: https://www.sciencedirect.com/science/article/pii/S0142061519334477.

[29] Mohamed H. Okba et al. "High voltage direct current transmission - A review, part I". In: *2012 IEEE Energytech*. 2012, pp. 1–7. DOI: 10.1109/EnergyTech.2012.6304650.

[30] Oluwafemi E. Oni, Innocent E. Davidson, and Kamati N.I. Mbangula. "A review of LCC-HVDC and VSC-HVDC technologies and applications". In: *2016 IEEE 16th International Conference on Environment and Electrical Engineering (EEEIC)*. 2016, pp. 1–7. DOI: 10.1109/EEEIC.2016.7555677.

[31] Fang Z. Peng. "Flexible AC Transmission Systems (FACTS) and Resilient AC Distribution Systems (RACDS) in Smart Grid". In: *Proceedings of the IEEE* 105.11 (2017), pp. 2099–2115. DOI: 10.1109/JPROC.2017.2714022.

[32] Dionisio Ramirez et al. "STATCOM Control Strategies". In: *Static Compensators (STATCOMs) in Power Systems*. Ed. by Farhad Shahnia, Sumedha Rajakaruna, and Arindam Ghosh. Singapore: Springer Singapore, 2015, pp. 147–186. DOI: 10.1007/978-981-287-281-4_5.

[33] David Rivera et al. “Power Grid Dynamic Performance Enhancement via STATCOM Data-Driven Control”. In: *Mathematics* 9.19 (2021). ISSN: 2227-7390. DOI: 10.3390/math9192361. URL: https://www.mdpi.com/2227-7390/9/19/2361.

[34] Abhinav Kumar Singh and Bikash C. Pal. “Chapter 1 - Introduction”. In: *Dynamic Estimation and Control of Power Systems*. Ed. by Abhinav Kumar Singh and Bikash C. Pal. Academic Press, 2019, pp. 1–8. ISBN: 978-0-12-814005-5. DOI: https://doi.org/10.1016/B978-0-12-814005-5.00012-1. URL: https://www.sciencedirect.com/science/article/pii/B9780128140055000121.

[35] Aastha Singhal, Charu Madhu, and Vijay Kumar. “Designs of All Digital Phase Locked Loop”. In: *2014 Recent Advances in Engineering and Computational Sciences (RAECS)*. 2014, pp. 1–5. DOI: 10.1109/RAECS.2014.6799523.

[36] Georgios Stamatiou. “Converter interactions in VSC-based HVDC systems”. PhD thesis. CHALMERS UNIVERSITY OF TECHNOLOGY, 2015, p. 208.

[37] “Two-level PWM VSC Converters”. In: *High Voltage Direct Current Transmission*. John Wiley & Sons, Ltd, 2019. Chap. 15, pp. 193–204. ISBN: 9781119566632. DOI: https://doi.org/10.1002/9781119566632.ch15. eprint: https://onlinelibrary.wiley.com/doi/pdf/10.1002/9781119566632.ch15. URL: https://onlinelibrary.wiley.com/doi/abs/10.1002/9781119566632.ch15.

[38] “Two-level VSC HVDC Modelling, Control, and Dynamics”. In: *High Voltage Direct Current Transmission*. John Wiley & Sons, Ltd, 2019. Chap. 17, pp. 227–245. ISBN: 9781119566632. DOI: 10.1002/9781119566632.ch17.

[39] Til Kristian Vrana and Sintef Energi. “Review of HVDC component ratings: XLPE cables and VSC converters”. In: *2016 IEEE International Energy Conference, ENERGYCON 2016* (2016). DOI: 10.1109/ENERGYCON.2016.7514045.

[40] Jan C Willems and Jan W Polderman. *Introduction to mathematical systems theory: a behavioral approach*. Vol. 26. Springer Science & Business Media, 1997.

[41] Jan C Willems et al. “A note on persistency of excitation”. In: *Systems & Control Letters* 54.4 (2005), pp. 325–329.

[42] Guanglu Wu et al. “Analysis and design of vector control for VSC-HVDC connected to weak grids”. In: *CSEE Journal of Power and Energy Systems* 3.2 (2017), pp. 115–124. DOI: 10.17775/CSEEJPES.2017.0015.

[43] Guozhou Zhang et al. “A data-driven approach for designing STATCOM additional damping controller for wind farms”. In: *International Journal of Electrical Power & Energy Systems* 117 (May 2020), p. 105620. DOI: 10.1016/j.ijepes.2019.105620.